Heterozygous loss of *WBP11* function causes multiple congenital defects in humans and mice

Ella M. M. A. Martin,[1] Annabelle Enriquez,[1,2] Duncan B. Sparrow,[1,3,4] David T. Humphreys,[5,2] Aideen M. McInerney-Leo,[6] Paul J. Leo,[7] Emma L. Duncan,[7,8,9] Kavitha R. Iyer,[1] Joelene A. Greasby,[1] Eddie Ip,[10,2] Eleni Giannoulatou,[10,2] Delicia Sheng,[1] Elizabeth Wohler,[11] Clémantine Dimartino,[12,13] Jeanne Amiel,[12,13,14] Yline Capri,[15] Daphné Lehalle,[16] Adi Mory,[17] Yael Wilnai,[17] Yael Lebenthal,[18,19] Ali G. Gharavi,[20] Grażyna G. Krzemień,[21] Monika Miklaszewska,[22] Robert D. Steiner,[23,24] Cathy Raggio,[25] Robert Blank,[26] Hagit Baris Feldman,[17,18] Hila Milo Rasouly,[20] Nara L. M. Sobreira,[11] Rebekah Jobling,[27] Christopher T. Gordon,[12,13] Philip F. Giampietro,[28] Sally L. Dunwoodie,[1,2,3] and Gavin Chapman[1,2*]

UNCORRECTED MANUSCRIPT

Downloaded from https://academic.oup.com/hmg/advance-article/doi/10.1093/hmg/ddaa258/6020188 by Bodleian Law Library user on 07 December 2020

© The Author(s) 2020. Published by Oxford University Press. All rights reserved. For Permissions, please email: journals.permissions@oup.com

[1] Development & Stem Cell Biology Division, Victor Chang Cardiac Research Institute, Sydney 2010, Australia

[2] Faculty of Medicine, UNSW Sydney 2052, Australia

[3] Faculty of Science, UNSW Sydney 2052, Australia

[4] Department of Physiology, Anatomy and Genetics, University of Oxford, Oxford OX1 3PT, UK

[5] Molecular, Structural and Computational Biology Division, Victor Chang Cardiac Research Institute, Sydney 2010, Australia

[6] Dermatology Research Centre, The University of Queensland Diamantina Institute, Translational Research Institute, Brisbane 4072, Australia

[7] Translational Genomics Group, Institute of Health and Biomedical Innovation, Faculty of Health, Queensland University of Technology, Translational Research Institute, Princess Alexandra Hospital, Ipswich Rd, Woolloongabba 4102, Australia

UNCORRECTED MANUSCRIPT

Downloaded from https://academic.oup.com/hmg/advance-article/doi/10.1093/hmg/ddaa258/6020188 by Bodleian Law Library user on 07 December 2020

[8] Department of Twin Research & Genetic Epidemiology, School of Life Course Sciences, Faculty of Life Sciences and Medicine, King's College London, SE1 7EH, UK

[9] Faculty of Medicine, University of Queensland, Herston 4006, Australia

[10] Computational Genomics Laboratory, Victor Chang Cardiac Research Institute, Sydney 2010, Australia

[11] McKusick-Nathans Department of Genetic Medicine, Johns Hopkins University, Baltimore 21287, USA

[12] Laboratory of Embryology and Genetics of Human Malformations, Institute National de la Santé et de la Recherche Médicale (INSERM) UMR 1163, Institut Imagine, Paris 75015, France

[13] Paris Descartes-Sorbonne Paris Cité Université, Institut Imagine, Paris 75015, France

[14] Département de Génétique, Hôpital Necker-Enfants Malades, Assistance Publique Hôpitaux de Paris, Paris 75015, France

[15] Département de Génétique, Hôpital Robert Debré, Assistance Publique Hôpitaux de Paris, Paris 75019, France

[16] Centre Hospitalier Intercommunal Créteil, Créteil 94000, France

[17] The Genetics Institute, Tel Aviv Sourasky Medical Center, Tel Aviv 6423906, Israel

[18] Sackler Faculty of Medicine, Tel Aviv University, Tel Aviv 6997801, Israel

[19] Dana-Dwek Children's Hospital, Tel Aviv Sourasky Medical Center, Pediatric Endocrinology and Diabetes Unit, Tel Aviv 6423906, Israel

[20]Department of Medicine, Division of Nephrology, Columbia University, New York 10032, USA

[21] Department of Pediatrics and Nephrology, Warsaw Medical University, Warsaw 02-091, Poland

[22] Department of Pediatric Nephrology and Hypertension, Jagiellonian University of Cracow, Kraków 30-663, Poland

[23] Marshfield Clinic Health System, Marshfield 54449, USA

[24] University of Wisconsin School of Medicine and Public Health, Madison 53792, USA

UNCORRECTED MANUSCRIPT

Downloaded from https://academic.oup.com/hmg/advance-article/doi/10.1093/hmg/ddaa258/6020188 by Bodleian Law Library user on 07 December 2020

[25] Hospital for Special Surgery, Pediatrics Orthopedic Surgery, New York 10021, USA

[26] Medical College of Wisconsin, Medicine, Milwaukee 53226, USA

[27]The Hospital for Sick Children, Division of Clinical and Metabolic Genetics, Toronto M5G1X3, Canada

[28]University of Illinois-Chicago, Department of Pediatrics, Chicago, Illinois 60607, USA

*To whom correspondence should be addressed at: Gavin Chapman, Victor Chang Cardiac Research Institute, Sydney, NSW, Australia. Tel: +61 (0)2 9295 8630. E-mail: g.chapman@victorchang.edu.au

UNCORRECTED MANUSCRIPT

Downloaded from https://academic.oup.com/hmg/advance-article/doi/10.1093/hmg/ddaa258/6020188 by Bodleian Law Library user on 07 December 2020

Abstract

The genetic causes of multiple congenital anomalies are incompletely understood. Here we report novel heterozygous predicted loss-of-function and predicted damaging missense variants in the *WBP11* gene, in seven unrelated families with a variety of overlapping congenital malformations including cardiac, vertebral, tracheo-oesophageal, renal and limb defects. *WBP11* encodes a component of the spliceosome with the ability to activate pre-mRNA splicing. We generated a *Wbp11* null allele in mouse using CRISPR-Cas9 targeting. *Wbp11* homozygous null embryos die prior to E8.5, indicating that *Wbp11* is essential for development. Fewer *Wbp11* heterozygous null mice are found than expected, due to embryonic and postnatal death. Importantly, *Wbp11* heterozygous null mice are small and exhibit defects in axial skeleton, kidneys and oesophagus, similar to the affected individuals, supporting the role of *WBP11* haploinsufficiency in the development of congenital malformations in humans. Loss-of-function *WBP11* variants should be considered as a possible cause of VACTERL association as well as isolated Klippel-Feil syndrome, renal agenesis or oesophageal atresia.

UNCORRECTED MANUSCRIPT

Downloaded from https://academic.oup.com/hmg/advance-article/doi/10.1093/hmg/ddaa258/6020188 by Bodleian Law Library user on 07 December 2020

Introduction

Congenital malformations affect 3-6% of live human births and are associated with higher rates of fetal demise (1). Malformations occur in isolation or in combination, aggravating the burden of disease on families and society. In 80% of cases, the underlying aetiology is unknown (2). A genetic diagnosis enables surveillance for other complications, recurrence prevention and targeted treatment.

Historically, pathogenic variants have been identified by studying families or groups of individuals who display similar phenotypic features that then typify a syndrome. Multiple congenital anomalies have been associated with pathogenic variants in pleiotropic genes involved in cellular processes such as pre-mRNA splicing (3), DNA stability (4, 5), gene expression (6, 7), or nicotinamide adenine dinucleotide (NAD) synthesis (8, 9). In the absence of a discernible syndromic diagnosis and three or more of vertebral (V), anal (A), cardiac (C), tracheo-oesophageal (TE), renal (R) or limb (L) anomalies occur in an individual, then a diagnosis of VACTERL association may be made (10). VACTERL association is epitomised by its diversity of clinical features and causative factors, most of which are still unknown. While cases of VACTERL association lack a syndromic diagnosis, genetic factors contribute to its causation (11-13).

Over the years, massively parallel sequencing has introduced new approaches to gene discovery, including the development of global communities sharing information about novel variants in uncharacterised genes, enabling identification of additional cases with variants in those genes and characterisation of associated phenotypic features.

Here, we present individuals from seven unrelated families, with anomalies in one or more organ, each found to have a predicted loss-of-function, truncating or predicted damaging missense variant in the WW Domain Binding Protein 11 (*WBP11*, MIM 618083)

UNCORRECTED MANUSCRIPT

Downloaded from https://academic.oup.com/hmg/advance-article/doi/10.1093/hmg/ddaa258/6020188 by Bodleian Law Library user on 07 December 2020

gene. Variants in *WBP11* have not previously been associated with human disease. WBP11 (also known as NpwBP, SIPP1, SNP70, PPP1R165) is a recognised component of the splicing machinery and colocalises with SC35 in nuclear speckles (14), the site of splicing assembly, storage and regulation (15). WBP11 copurifies with complex B as part of the PRP19 complex of the spliceosome (16, 17), a dynamic ribonucleoprotein (RNP) complex responsible for the removal of non-coding segments, exon ligation (coding segments) and regulation of differential/alternative splicing of precursor mRNA (18). We targeted the *Wbp11* locus in mouse, confirming a link between *WBP11* loss-of-function and congenital disease. Our findings indicate *WBP11* haploinsufficiency causes a pleiotropic malformation syndrome affecting the cardiac, skeletal, gastrointestinal and renal systems.

Results

Predicted damaging *WBP11* variants are the top candidates for disrupting embryogenesis in patients with related developmental anomalies

Through exome sequencing by several groups investigating patient cohorts with vertebral malformations, syndromic oesophageal atresia, renal hypodysplasia or multiple congenital anomalies (see Supplemental Note: Case Reports), novel predicted damaging variants in the *WBP11* gene were identified independently as the variant most likely to cause disease. Phenotypic and mutational comparisons were subsequently facilitated via GeneMatcher (19).

Novel variants predicted to truncate WBP11 were identified in two unrelated families (Families 1 and 2, Table 1) through exome sequencing of an extended vertebral malformation cohort. Patient 3 had clinical trio exome sequencing to determine the cause of his multiple congenital anomalies. The predicted truncating variant in Family 4 was identified as part of an ongoing effort to determine the causes of syndromic forms of oesophageal atresia. Patients 5 and 6 were from a cohort of patients with renal hypodysplasia. Patient 7 and her unaffected

UNCORRECTED MANUSCRIPT

Downloaded from https://academic.oup.com/hmg/advance-article/doi/10.1093/hmg/ddaa258/6020188 by Bodleian Law Library user on 07 December 2020

mother underwent exome sequencing to investigate her congenital anomalies, short stature and microcephaly. In total, 13 affected individuals from seven unrelated families had a *WBP11* variant considered as the top candidate in each case. Each of these variants is absent from population databases. Of these, five *WBP11* variants are predicted to be truncating, four of which are expected to result in loss-of-function (LoF) alleles as transcripts including them will be subject to exon junction complex (EJC)-promoted nonsense-mediated decay (20). LoF variants in *WBP11* are underrepresented in the gnomAD database (probability of being LoF intolerant, pLI, score = 1, with 1 LoF variant observed and 32 expected) (21), consistent with the hypothesis that heterozygous LoF *WBP11* alleles are pathogenic. Transcripts including the c.1559dup p.(Gly521TrpfsTer28) variant (Patient 3) should escape EJC-promoted nonsense-mediated decay as the variant is in the final exon (Figure 1A), and therefore are likely to express a WBP11 protein lacking 121 amino acids from the C-terminus. Finally, Patient 6 harbours a novel missense variant c.169A>G p.(Met57Val), which is predicted to be damaging by CADD and Polyphen-2 metrics (Table S1). A methionine at this position in WBP11 orthologues is conserved in mammals, amphibians and fish.

The inheritance of *WBP11* variants from the apparently unaffected mother in Family 1 indicates that heterozygous LoF alleles are a partially penetrant cause of disease (Figure S1). Patients 1A and 1B had different phenotypic features and affected members of Family 4 had even more variable phenotypic expression, ranging from minor dysmorphology in the mother to major malformations resulting in fetal demise. Despite harbouring the same frameshift *WBP11* variant, affected individuals in Families 5 and 7 exhibited a variety of clinical presentations. Patient 5 only had renal agenesis reported, whereas Patient 7 had normal renal imaging but instead had cerebral, cardiac, tracheo-oesophageal and vertebral malformations. Again demonstrating variable disease expression even within the same

UNCORRECTED MANUSCRIPT

Downloaded from https://academic.oup.com/hmg/advance-article/doi/10.1093/hmg/ddaa258/6020188 by Bodleian Law Library user on 07 December 2020

family, her sister Patient 7A had duodenal atresia and Sprengel deformity. Two other sisters in Family 7 were also found to be heterozygous for the *WBP11* variant (Figure S1), and are awaiting investigations for malformations. The *WBP11* variant did not segregate with the unaffected mother in Family 7, and paternal DNA was not available. Inheritance in Family 7 might be presumed paternal, and indeed might explain the report of short stature and short neck in the father and his brother. Parental DNA was not available in Families 5 and 6 to determine variant inheritance. Patients 2 and 3 had *de novo WBP11* variants.

Following identification of predicted damaging *WBP11* variants in these families, each group independently screened our respective research cohorts for similar variants in *WBP11*. Among our cohorts of patients with vertebral malformation, syndromic oesophageal atresia, renal hypodysplasia, or multiple congenital anomalies, one additional *WBP11* variant was detected in a patient with Klippel-Feil syndrome. The *WBP11* insertion variant (c.191-2_191-1insAA) in this patient is in the splice acceptor site but does not modify the splice acceptor dinucleotide and is not predicted to alter *WBP11* splicing according to SpliceAI (22), Spliceogen (23) and maxEntScan (24); it is found in one individual in the gnomAD database. This patient also has a nonsense variant in the *KIAA1217* gene (NM_019590:c.4219A>T p.(Lys1407Ter)), which is considered the more likely genetic cause (25).

Patients with predicted LoF, truncating or damaging missense *WBP11* variants had overlapping phenotypes involving the heart, vertebrae, trachea, oesophagus, kidney, and limbs (Table 1). Short stature and/or decreased body weight were reported in five cases. Eight individuals from six families had congenital heart disease. Ventricular septal defect was the most common, occurring as an isolated finding in three cases and as part of a complex heart defect in Patients 3, 4A and 7. Patient 1B had self-resolved pulmonary stenosis and Patient 6 had an atrial septal defect. All the patients who have had vertebral imaging had

Downloaded from https://academic.oup.com/hmg/advance-article/doi/10.1093/hmg/ddaa258/6020188 by Bodleian Law Library user on 07 December 2020

UNCORRECTED MANUSCRIPT

abnormal vertebral morphology. These were identified in five families, presenting as fused cervical vertebrae and/or thoracic butterfly vertebrae in four individuals, and as a hypoplastic first costal arch in Patient 4D (Figure 1B-E). Patient 1A also had bilateral omovertebral bones and scapular elevation, with a short neck and low posterior hairline associated with his cervical vertebrae fusion. Patient 1B had congenital scoliosis while Patient 2 had associated abnormality of the ribs. Patient 7 had abnormal L5 vertebra (undefined) while her sister, Patient 7A, had Sprengel deformity. Additionally, Patients 4B and 4D had Sprengel deformity (Figure S3). Oesophageal atresia with tracheo-oesophageal fistula was found in Families 3, 4, 6, and 7, affecting six individuals in total. Patients 3 and 7A had duodenal atresia. Abnormal renal morphology was found in five cases from four families, the most severe being renal agenesis in Patients 4C, 5 and 6. Limb abnormalities were identified in five cases from three families. Notably, Patient 3 had hypoplasia of the left thumb (Figure S2), and Family 4 had three members with a range of anomalies including tapered fingers, camptodactyly and hypoplasia of the thumb (Figure S3). Patient 1A had clinodactyly of the fifth finger. Dysmorphic facial features were not constant but include facial asymmetry, reported in Patients 1A and 4D. Features reported in single cases include choanal atresia, submucous cleft palate with velopharyngeal insufficiency and conductive hearing impairment, broad forehead with deeply set eyes, hypertrichosis, low-set dysplastic ear with retrognathia, preauricular pit, preauricular skin tags, cryptorchidism and inguinal hernia. In Family 4, head circumferences (HC) measured from early childhood were at least two standard deviations (SD) below the mean, including that of the mother; but HC measured before term gestation ranged between –1.5 to 0 SD from the mean. Growth parameters of Patient 6 were all more than two SD below the mean. Patient 7 had microcephaly with agenesis of the corpus callosum and short stature. Patient 2 had both microcephaly and chromosome 1q21.1 deletion in common with her mother, who had no other anomalies. This

UNCORRECTED MANUSCRIPT

Downloaded from https://academic.oup.com/hmg/advance-article/doi/10.1093/hmg/ddaa258/6020188 by Bodleian Law Library user on 07 December 2020

374 kilobase deletion does not include disease-associated genes and does not overlap with the recognised 1.35 megabase microdeletion in chromosome 1q21.1 (MIM 612474) (26) (see Supplemental Note: Case Reports). Moreover, Patient 2 was delayed in achieving her developmental milestones, Patient 3 had mild intellectual disability (ID), Patient 1B had suspected attention deficit hyperactivity disorder (ADHD), and Patient 7 had global developmental delay (DD) and ADHD. Limited information regarding extra-renal manifestations was available for Patients 5 and 6. Ophthalmological features were not reported in any of the patients. There was no documented history of antenatal teratogen exposure. Patients 1A, 3, 4D, 5, 6 and 7 had a normal chromosome microarray and Patients 3 and 4D also had normal chromosome breakage studies.

Given that vertebral defects were common in patients identified with *WBP11* variants, we investigated if a cohort of vertebral malformation patients harboured an enrichment in *WBP11* variants compared with controls. Rare variant enrichment analysis (27) was carried out, testing for enrichment in the number of *WBP11* variants in exome data of 58 vertebral malformation patients compared with 194 control exomes that passed quality control. Variation in *WBP11* was significantly enriched in the vertebral malformation cohort compared with controls, either when considering all coding variants (except synonymous SNVs) and splicing variants (Table 2, Set1, $p = 0.01911$) or when only predicted damaging variants were included (Table 2, Set2, $p = 0.02032$).

Wbp11 heterozygous null mice model variable penetrance and expressivity observed in patients

To link the *WBP11* predicted LoF variants identified in the affected individuals with the constellation of their organ defects, we generated a *Wbp11* null allele in mice using CRISPR-Cas9. Since targeting C57BL/6J zygotes was unsuccessful, exon 5 was targeted on

Downloaded from https://academic.oup.com/hmg/advance-article/doi/10.1093/hmg/ddaa258/6020188 by Bodleian Law Library user on 07 December 2020

UNCORRECTED MANUSCRIPT

an FVB/N × C57BL/6J F1 hybrid background generating a single founder carrying an 8 bp deletion, causing premature termination of the protein six amino acids downstream (Figure S4A). This site is 8 bp away from the equivalent position of variant c.280C>T p.(Arg94Ter) identified in Family 1.

In some families with putative heterozygous LoF variants there is incomplete penetrance and variable expressivity. The same variability is seen in the mouse model. Mice carrying the *Wbp11* null allele were not found in the expected Mendelian ratio in progeny from *Wbp11*$^{+/+}$ × *Wbp11*$^{+/-}$ matings with only a third of live mice being heterozygous null post-weaning (Figure 2A, p = 0.0001). *Wbp11*$^{+/-}$ mice were also underrepresented at P12 and at E17.5, indicating that a proportion of *Wbp11*$^{+/-}$ mice died during gestation and shortly after birth (Figure 2A, E17.5 p = 0.0263, P12 p = 0.0412). The percentage of *Wbp11*$^{+/-}$ mice that died increased with subsequent backcrosses onto C57BL/6J or FVB/N strains (Figure S4C-F), presumably because heterosis (hybrid vigour) of the FVB/N × C57BL/6J hybrid founder is lost through successive backcrosses to inbred strains. Significantly more male *Wbp11*$^{+/-}$ mice died or needed to be culled on either background compared to *Wbp11*$^{+/-}$ females (Figure 2B, FVB/N p = 0.0063, C57BL/6J p = 0.0049). Because the partial lethality of the *Wbp11* null allele worsened as the mice were backcrossed to inbred FVB/N and C57BL/6J strains, subsequent skeletal and internal soft tissue analysis was restricted to the second FVB/N backcross and comparisons made to wildtype littermates.

E17.5 *Wbp11*$^{+/-}$ embryos weighed 30% less on average than their wildtype littermates (Figure 2C, p<0.0001) and exhibited the appropriate developmental landmarks (wrinkled skin, disappearance of umbilical hernia, and parallel fingers and toes), indicating that their reduced weight was not due to developmental delay (Figure 2D). Even though placentas of *Wbp11*$^{+/-}$ embryos weighed 10% less than those of *Wbp11*$^{+/+}$ embryos (Figure 2E, p =

UNCORRECTED MANUSCRIPT
Downloaded from https://academic.oup.com/hmg/advance-article/doi/10.1093/hmg/ddaa258/6020188 by Bodleian Law Library user on 07 December 2020

0.0239), the ratio of fetal weight to placental weight was 22% lower in *Wbp11*$^{+/-}$ embryos compared to wildtype littermates, suggesting either an inherent growth defect in the embryo or that *Wbp11* heterozygosity impaired placental efficiency (Figure 2F, $p<0.0001$).

Given that a proportion of *Wbp11*$^{+/-}$ mice died postnatally, we hypothesised that embryos homozygous null for *Wbp11* may not be viable. To test this, we carried out *Wbp11*$^{+/-}$ × *Wbp11*$^{+/-}$ matings and harvested embryos at E8.5. *Wbp11*$^{+/-}$ embryos at this stage had rounded head folds and it was difficult to discern their somites, indicative of a slight delay in development (~half a day) compared to wildtype littermates (Figure 2H). *Wbp11* homozygous null embryos were not found at E8.5 (Figure 2G, $p = 0.0007$), indicating that *Wbp11* is an essential gene for development.

Wbp11 **heterozygous mutant mice display several axial skeletal defects**

Of the families reported here, most had skeletal abnormalities including cervical vertebral fusions and rib abnormalities. To determine if the same was true in mice, we assessed the skeletons of *Wbp11*$^{+/-}$ mice at P12 by micro-CT. All seven *Wbp11*$^{+/-}$ pups analysed had cervical vertebral fusions reminiscent of those seen in many of the affected individuals (Figure 3, Table S2 $p<0.0001$). Other cervical defects seen in *Wbp11*$^{+/-}$ mice include absent vertebral elements, asymmetry of the midline, hemi- and butterfly vertebrae, cervical ribs, hypoplastic transverse processes and dyssymphysis. Rib defects (small or absent 13th rib) and sternum malformations (fusions between the 3rd and 4th sternebrae) were also common (Table S2, $p<0.0001$). The majority of *Wbp11*$^{+/-}$ pups had five lumbar vertebrae rather than the usual six (Table S2, $p<0.0001$). Fewer defects were found in the thoracic region with two *Wbp11*$^{+/-}$ pups having fused vertebrae (Figure 3D) and another having hypoplastic transverse processes in two thoracic vertebrae. No defects were observed

Downloaded from https://academic.oup.com/hmg/advance-article/doi/10.1093/hmg/ddaa258/6020188 by Bodleian Law Library user on 07 December 2020

UNCORRECTED MANUSCRIPT

in sacral and caudal regions. Thus, *WBP11* haploinsufficiency causes axial skeletal defects in humans and mouse, most commonly in the cervical vertebrae.

***Wbp11* heterozygosity affects multiple organ systems**

To detect defects in organs and other tissues, we stained E17.5 embryos with Lugol's reagent and performed contrast-enhanced micro-CT, which captures soft tissue anatomy (28). All ten *Wbp11*$^{+/-}$ embryos examined had oedema in the head (Table S3, p<0.0001) with associated reduced brain volume (Figure 2D, 4A). Volume measurements of the brain confirmed that *Wbp11*$^{+/-}$ embryos had on average a 24% smaller brain than wildtype littermates (Figure 4B, p<0.0001). To evaluate the extent of the reduction, we measured brain anteroposterior (AP) length, cortical width and cortical thickness from 3D micro-CT reconstructions (Figure 4C) (29, 30). All 3 measurements were significantly lower in the *Wbp11*$^{+/-}$ embryos compared to wildtype littermates (Figure 4D-F, D p = 0.004, 4E-4F p<0.0001), indicating that brain size is reduced but otherwise appeared normal in *Wbp11* heterozygotes.

Wbp11$^{+/-}$ mouse embryos also had kidney and lung defects at E17.5. In four out of ten *Wbp11*$^{+/-}$ embryos the kidneys appeared smaller and abnormally elongated (Figure 5A, Table S3 p = 0.019). Volume measurements confirmed that both left and right kidneys were 30% smaller in *Wbp11*$^{+/-}$ embryos compared to wildtype littermates (Figure 5A, left kidney p = 0.0024, right kidney p = 0.0002). Although smaller than wildtype, kidneys from *Wbp11*$^{+/-}$ embryos were structurally normal (Figure 5B). The lungs were also significantly smaller in *Wbp11*$^{+/-}$ embryos compared to wildtype littermates (Figure 5C p = 0.0034). Unlike affected individuals, heart defects, tracheo-oesophageal fistula or oesophageal atresia were not observed in *Wbp11*$^{+/-}$ embryos. However, a small blind sac attached to the oesophagus was

Downloaded from https://academic.oup.com/hmg/advance-article/doi/10.1093/hmg/ddaa258/6020188 by Bodleian Law Library user on 07 December 2020

UNCORRECTED MANUSCRIPT

found near the stomach in two of the ten *Wbp11*$^{+/-}$ embryos examined (Figure S5, Table S3). No obvious craniofacial or stomach defects were found when analysing E17.5 embryos. However, internal analysis of the head revealed that three out of ten *Wbp11*$^{+/-}$ embryos had unilateral choanal atresia (Figure S5, Table S3), an anomaly also found in Patient 2. Even though there were no obvious defects in the liver, volume analysis revealed that *Wbp11*$^{+/-}$ embryos had significantly smaller livers compared to wildtype littermates (Figure 5D p = 0.0001). We also examined *Wbp11*$^{+/-}$ embryos from later FVB/N backcrosses (backcross 3), which exhibit higher rates of postnatal death, at E15.5 in an attempt to detect defects responsible for embryo death by E17.5. Like E17.5 *Wbp11*$^{+/-}$ embryos from an earlier backcross, E15.5 embryos had oedema (Table S4 p = 0.01), choanal atresia (Table S4 p = 0.01) and a blind sac arising from the oesophagus (Table S4 p = 0.049), but heart defects and more severe oesophageal defects were not found (Figure S6, Table S4). Three out of eight *Wbp11*$^{+/-}$ embryos at E15.5 had severe cleft palate, a defect not observed in E17.5 *Wbp11*$^{+/-}$ embryos, suggesting that the palate fuses by E17.5 in such embryos or that they die before E17.5 (Table S4, p = 0.049).

Given the presence of tissue specific defects in *Wbp11*$^{+/-}$ embryos, we sought to establish the expression pattern of WBP11 during development. A polyclonal anti-WBP11 antibody specifically detected transfected FLAG-WBP11 as well as endogenous WBP11 at the expected size of 90 kDa in mouse E9.5 embryo lysates (Figure 6A) (14). Anti-WBP11 reactivity was largely nuclear in E9.5 mouse embryos, where it was found in the presomitic mesoderm and somites, the progenitors of the vertebrae and all other tissues at this stage, although expression was higher in the surface ectoderm and in fetal blood cells (Figure 6B). WBP11 was also ubiquitously expressed at stages E10.5, E11.5 and E12.5 (Figure 6C-K, not

Downloaded from https://academic.oup.com/hmg/advance-article/doi/10.1093/hmg/ddaa258/6020188 by Bodleian Law Library user on 07 December 2020

UNCORRECTED MANUSCRIPT

shown). Thus, WBP11 protein expression is not restricted to precursors of tissues affected by *Wbp11* heterozygosity.

Discussion

WBP11 is an established component of the spliceosome that activates pre-mRNA splicing(14, 31-33). Here we report novel predicted LoF and missense variants in the *WBP11* gene in at least 13 individuals from seven families exhibiting an overlapping range of phenotypes including vertebral, cardiac, oesophageal and renal defects. We also report that *Wbp11*$^{+/-}$ mouse embryos exhibit anomalies that overlap with those found in affected individuals.

Transcripts from truncating *WBP11* alleles found in the affected individuals, with the exception of c.1559dup p.(Gly521TrpfsTer28), are likely to undergo nonsense-mediated decay and therefore express little or no truncated protein. Consistent with this, *Wbp11* expression in *Wbp11*$^{+/-}$ mice was approximately half (0.53x) that of wildtype littermates (Figure S4B, $p = 0.008$). Even if truncated WBP11 proteins were to be expressed from alleles found in patients, they are expected to lack the ability to activate splicing since they are shorter than those previously shown to lack splicing activity (33). Thus the variants described in this study that are predicted to truncate WBP11 are likely to create LoF alleles.

Several additional lines of evidence support the hypothesis that predicted LoF *WBP11* variants cause congenital disease. Firstly, we confirm an association between *WBP11* variation and congenital disease by demonstrating that predicted damaging variants in *WBP11* are significantly enriched in a cohort of patients with vertebral malformations, compared with controls. Secondly, mice heterozygous for a *Wbp11* null allele exhibit cervical vertebral, renal and oesophageal defects like patients carrying heterozygous predicted LoF *WBP11* variants. Finally, *WBP11* is among those genes that are intolerant to LoF variation, a

Downloaded from https://academic.oup.com/hmg/advance-article/doi/10.1093/hmg/ddaa258/6020188 by Bodleian Law Library user on 07 December 2020

UNCORRECTED MANUSCRIPT

group that includes almost all known human haploinsufficient disease genes (34). Thus, the phenotype described in the affected patients is likely caused by haploinsufficiency of *WBP11*. Taken together, our findings indicate LoF variants in *WBP11* are a cause of congenital anomalies in humans and in mice.

The American College of Medical Genetics and Genomics (ACMG) and Association for Molecular Pathology (AMP) guidelines (35, 36) do not apply to initial reports of novel gene-disease associations. However, once the link between the *WBP11* LoF variants and congenital anomalies reported here is recognised, we would be able to interpret the variants reported here using these guidelines. With the exception of c.169A>G p.(Met57Val), the novel predicted LoF variants would then receive a pathogenic or likely pathogenic ACMG-AMP classification.

While *WBP11* has not previously been associated with disease, mutation of its binding partner *PQBP1* (MIM 300463) causes Renpenning syndrome (MIM 309500)(37). Clinical features in affected patients include ID, microcephaly, short stature, small testes and less commonly, dysmorphic facial features, cleft palate and congenital heart defects (37, 38). Like WBP11, PQBP1 is a splicing factor (39) but unlike WBP11, it has roles in innate immunity (40) and neurodegeneration (41). Notably, the c.194A>G p.(Y65C) variant in *PQBP1*, a cause of Renpenning syndrome (42), disrupts WBP11 binding to PQBP1 and reduces pre-mRNA splicing in patient lymphoblasts (43). Thus, there may be common aspects to the aetiology of both diseases that includes disruption of splicing.

WBP11 and *PQBP1* have important roles during early development in Xenopus. Morpholino knockdown of *wbp11* in *Xenopus* embryos causes anteroposterior axis truncation and small or absent heads and tails, phenotypes similar to *pqbp1* knockdown (44). While we do not have complete growth data for our cohort, growth restriction has been reported in some of the affected individuals. *WBP11* knockdown caused reduced expression of

UNCORRECTED MANUSCRIPT

Downloaded from https://academic.oup.com/hmg/advance-article/doi/10.1093/hmg/ddaa258/6020188 by Bodleian Law Library user on 07 December 2020

mesoderm markers *wnt8*, *fgf4* and *cdx4* but not the pan-mesoderm marker *brachyury* (44). Our findings demonstrate a developmental role for *Wbp11* in mammals, with partial embryonic and postnatal lethality, axial skeletal, renal and oesophageal defects and reduced brain and organ volumes evident in heterozygous null mouse embryos and early embryonic lethality (prior to E8.5) of homozygous null embryos. Abnormal mesoderm specification in *Wbp11* heterozygous null embryos may be responsible for defects in the axial skeleton and kidneys.

Phenotypes reported here for *WBP11* overlap those associated with variants in other spliceosomal genes: choanal atresia and cardiac malformations are features of Burn-McKeown syndrome (MIM 608572) caused by the variants in the splicing factor *TXNL4A* (MIM 611595)(45); renal, cardiac and vertebral anomalies are found in some patients with cerebrocostomandibular syndrome (MIM 117650) caused by *SNRPB* (MIM 182282) mutation (46, 47); cardiac, renal and skeletal anomalies are reported in patients with Verheij syndrome (MIM 615583) due to pathogenic variants in *PUF60* (MIM 604819)(3, 48), and vertebral and cardiac malformations are features of Au-Kline syndrome (MIM 616580) due to pathogenic variants in *HNRNPK* (MIM 600712)(49). A homozygous likely pathogenic variant in *CDK9* (MIM 603251), an important player in alternative RNA splicing (50), has been reported in families sharing similar features of cardiac, renal and skeletal anomalies, as well as microcephaly, coloboma and cataracts(51). Interestingly, WBP11 interacts with EFTUD2 (MIM 603892)(52), variants in which cause mandibulofacial dysostosis with oesophageal atresia and renal anomalies (MIM 610536)(53, 54). Perhaps most similar to the defects reported here for *WBP11* heterozygosity are those caused by truncating variants in the spliceosome component *SON* (MIM 182465), which cause ZTTK syndrome (MIM 617140) characterised by ID and congenital anomalies affecting the brain, heart, kidney, vertebrae and ribs (55, 56). Unlike other diseases caused by mutation of splicing genes (57), patients with

UNCORRECTED MANUSCRIPT

Downloaded from https://academic.oup.com/hmg/advance-article/doi/10.1093/hmg/ddaa258/6020188 by Bodleian Law Library user on 07 December 2020

predicted damaging variants in *WBP11* do not have overt eye anomalies, although they have not all undergone ophthalmological assessment, and ID is not common. Thus, disease caused by disruption of *WBP11* has overlapping but distinct features compared with known diseases of this class.

There is considerable variation in the penetrance and expressivity of defects found within families and between families with distinct *WBP11* variants. Incomplete penetrance in families with congenital vertebral segmentation defects and congenital heart disease is a recognised phenomenon(58-61). In Family 1, the variant was inherited from the apparently unaffected mother, while the inheritance in Families 5 and 6 is unknown. In Family 7, two of the sisters with the *WBP11* variant are yet to demonstrate a phenotype, pending organ imaging. Different phenotypic features are present in the affected individuals from Families 1,4 and 7. There was limited assessment of extra-renal phenotypes for Patients 5 and 6 as they were ascertained from nephrology services, and it is possible that these patients have additional malformations in common with the rest of the cohort. Given their diverse phenotypes, the patients in our study would not have been considered collectively to have a unifying genetic cause if it was not for the collaborative investigation established via GeneMatcher (19). Nonetheless, most families shared a combination of vertebral, cardiac, gastrointestinal and/or renal malformations. Consistent with predicted damaging *WBP11* variants causing these phenotypes, such variants are significantly enriched in our cohort of patients with vertebral malformation.

The combination of malformations detected in the affected individuals overlap those described in VACTERL association (MIM 192350) with at least five of the patients affected with features in three component organs (10, 62). LoF *WBP11* variants should be considered when seeking a genetic aetiology for patients who fall under the broad spectrum of VACTERL association, even in those who have less than three organs affected. Indeed,

Downloaded from https://academic.oup.com/hmg/advance-article/doi/10.1093/hmg/ddaa258/6020188 by Bodleian Law Library user on 07 December 2020

UNCORRECTED MANUSCRIPT

family studies have identified component organ abnormalities in first-degree relatives of individuals with VACTERL association, and vertebral malformations are the most prevalent (11, 63). The variable phenotypic expression within the affected families is consistent with this observation. *WBP11* should also be considered in cases that include Klippel-Feil syndrome, renal agenesis or oesophageal atresia. Identification of the disease-causing variant enables reverse phenotyping, which may uncover other abnormalities similar to those reported here.

Vertebral and renal anomalies are common between *WBP11* patients and *Wbp11* heterozygous null mice, confirming *Wbp11* mutation as a cause of congenital defects and consistent with our hypothesis that LoF variants in *WBP11* lead to congenital disease in humans. Oesophageal atresia with tracheo-oesophageal fistula was not observed although minor oesophageal defects are present in *Wbp11* heterozygous null mice. Likewise, congenital heart defects observed in eight of the cases were not found in our mouse model. While we noted some loss of *Wbp11*$^{+/-}$ embryos prior to E17.5 that could be caused by heart abnormalities, we found no evidence of heart defects earlier in development at E15.5. We found that WBP11 expression was not restricted to affected tissues and organs or their progenitors and instead was ubiquitous at the stages of mouse development examined. Abnormalities unique to the mouse model include oedema, hypoplastic ectopic thymii, small lungs and liver. A narrow and elongated snout was observed in some *Wbp11* heterozygous null mice (not shown), although this was not evident at E17.5. We also noted that some *Wbp11* heterozygous null mice ran in circles, suggestive of vestibular dysfunction (not shown).

It is not uncommon for the phenotypes observed in knockout mouse lines to diverge from the human disease that they are intended to model. A study by the International Mouse Phenotyping Consortium (IMPC) showed that only 40% of IMPC mouse lines orthologous to

UNCORRECTED MANUSCRIPT

Downloaded from https://academic.oup.com/hmg/advance-article/doi/10.1093/hmg/ddaa258/6020188 by Bodleian Law Library user on 07 December 2020

rare disease-gene associations had one or more phenotypes in common with the human disease (64). Phenotypes of mice carrying null alleles do not always correlate well when comparing among multiple genetic backgrounds (65), providing one possible explanation for the observed divergence between reported phenotypes in mouse and those of patients. Our own data indicate that, like the affected individuals, *Wbp11* heterozygous mice exhibit variable penetrance and expressivity. Postnatal survival of *Wbp11* heterozygous mice also differed between the two genetic backgrounds we examined. Given the variability observed among individual mice and backgrounds, it is not surprising that there are some differences in organs/tissues affected in *Wbp11* heterozygous mice and patients with predicted LoF heterozygous variants in *WBP11*.

Wbp11 heterozygous null mouse embryos have reduced brain volume compared to wildtype littermates but no obvious structural brain anomalies, suggestive of a primary microcephaly (66). It is interesting to note that *PQBP1* variants cause primary microcephaly in patients without structural disruption to the brain (67). In patients with *WBP11* variants, head circumference was reduced in several individuals: affected individuals in Family 4 had reduced head circumference postnatally and Patients 6 and 7 had growth parameters under the 3rd centile. Microcephaly in Patient 2 and her otherwise unaffected mother may be due to their shared 1q21.1 microdeletion, but the *de novo WBP11* variant may have also been contributory. Further work will be required to establish a link between *WBP11* mutation and microcephaly.

WBP11 was listed among 3435 candidate developmental lethal genes in mouse that were not yet linked to human disease (68). Here, we report that heterozygous predicted LoF *WBP11* variants cause an overlapping constellation of congenital malformations in humans, and in mice, loss of *Wbp11* does indeed cause early embryonic lethality. Moreover, fetal and postnatal death of heterozygous null mice is a feature of our *Wbp11* mouse model. In this

Downloaded from https://academic.oup.com/hmg/advance-article/doi/10.1093/hmg/ddaa258/6020188 by Bodleian Law Library user on 07 December 2020

UNCORRECTED MANUSCRIPT

regard, an instance of fetal demise at 16 weeks was recorded in Family 4 in our cohort, raising the possibility that *WBP11* heterozygosity also causes partial lethality during development and neonatally in humans. In general, partial lethality in the heterozygous state is not common in mice. Of the 2252 mouse knock-out lines reported thus far that show prenatal lethality, only 203 exhibit lethality in the heterozygous state. This is perhaps due to difficulties targeting and breeding such lines. A null allele in the gene for WBP11's binding partner PQBP1 reportedly cannot be generated (44), suggesting that it has an essential cellular function. *Wbp11* is also considered essential for cell viability (68) and our attempts to target the *Wbp11* locus with CRISPR-Cas9 failed on the C57BL6/J background with targeting on a F1 hybrid background necessary to generate the allele. Consistent with this, on the inbred C57BL6/J background, half of the *WBP11* heterozygous null mice die or are culled due to hydrocephalus.

In sum, we report predicted LoF variants in the splicing factor gene *WBP11* cause a phenotype characterised by vertebral, cardiac, tracheo-oesophageal, renal, and limb malformations. Follow-up studies will be required to further define the function of WBP11 and its role in the pathogenesis of the developmental anomalies reported here. Recognition of *WBP11* as an essential developmental gene will enable identification of pathogenic variants in more patients with single or multiple congenital anomalies, improving our ability to provide more accurate recurrence risks and guide surveillance for possible complications in affected families. Conversely, identification of pathogenic *WBP11* variants in more patients will extend the phenotypic spectrum related to *WBP11* in humans, potentially establishing its association with microcephaly and other organ anomalies.

UNCORRECTED MANUSCRIPT

Downloaded from https://academic.oup.com/hmg/advance-article/doi/10.1093/hmg/ddaa258/6020188 by Bodleian Law Library user on 07 December 2020

Materials and Methods

DNA samples, exome sequencing and variant analysis

Families 1 to 4 and 7 were ascertained through Medical Genetics services, and Families 5 and 6 through Nephrology services. Families 1 and 2 were included in a cohort of 76 probands with segmentation defects of the vertebrae that underwent family-based exome sequencing and analysis. Family 3 underwent clinical trio exome sequencing. Family 4 was part of a cohort of families with syndromic oesophageal atresia. Families 5 and 6 were enrolled in a case-control study that compared 525 patients with renal hypodysplasia recruited from Nephrology clinics and 6585 controls. Family 7 was part of a cohort of 200 trio exomes, where each proband fulfilled one of the following criteria for inclusion: a. severe global DD/ ID - developmental quotient/intelligence quotient (DQ/IQ) <54; b. mild-moderate global DD/ ID - DQ/IQ <70 and major anomaly or seizures; or c. two congenital major anomalies. Investigations were performed after obtaining informed consent in accordance with the ethics standards of the responsible institutional review boards. Exome sequencing and variant analysis for each family are described in the Supplement.

Rare variant enrichment analysis

Exome data from 76 probands with vertebral malformations and 200 controls (Osteoporosis cases provided by Anglo-Australasian Osteoporosis Genetics Consortium) were considered for rare variant enrichment analysis. Application of Principal Component Analysis and Sample quality control metrics were applied as described in (69) reducing vertebral case samples to 58 and control samples to 194. Rare variants (MAF <0.01) were considered disruptive (nonsense, frameshift and essential splice-site variants) or missense variants rated as predicted damaging by two prediction algorithms (PolyPhen-2 HVAR and

UNCORRECTED MANUSCRIPT

Downloaded from https://academic.oup.com/hmg/advance-article/doi/10.1093/hmg/ddaa258/6020188 by Bodleian Law Library user on 07 December 2020

CADD Phred). Enrichment analyses were performed on these variants sets using SNP-set (Sequence) Kernel Association Test-Optimised (SKAT-O) test (27) to determine association of variant burden.

Generation of *Wbp11* null mice and genotyping

CRISPR targeting of the *Wbp11* locus was carried out by the MEGA team at Australian BioResources (Moss Vale, NSW, Australia). Single guide RNA (AAGGCGTAGAATGCGTTCAA) was designed against exon 5 of *Wbp11* with the aim of creating a frameshift mutation to disrupt protein function. Electroporation of CRISPR guide RNA/Cas9 into C57BL/6J / FVB/N F1 zygotes generated a single founder carrying an allele with an 8 bp deletion which was successfully passed on to the next generation. This deletion causes a reading frameshift and termination of the protein six amino acids downstream (Figure S4A). The genotyping strategy utilises the fact that the 8 bp deletion removes a XmnI restriction site to distinguish the wildtype and null *Wbp11* alleles following PCR amplification of exon 5 (Forward primer: TGGGTCACTTCTGGGAACGA; Reverse primer: TCACGCTCTTACTCATGTTTACCA).

Breeding and timed matings

This research was performed following the guidelines, and with the approval, of the Garvan Institute of Medical Research/St. Vincent's Animal Experimentation Ethics Committee, research approvals 15/27 and 18/27. Since C57BL/6J mice are predisposed to developing hydrocephalus (70), the founder and subsequent male heterozygous *Wbp11* mutant offspring were backcrossed to FVB/N females to maintain the colony. Mice were examined for vaginal plugs in the morning and the presence of a plug was taken as embryonic day 0.5 (E0.5). Pregnant females were sacrificed at E8.5, E15.5 or E17.5, and

UNCORRECTED MANUSCRIPT

Downloaded from https://academic.oup.com/hmg/advance-article/doi/10.1093/hmg/ddaa258/6020188 by Bodleian Law Library user on 07 December 2020

uteri were examined for evidence of resorptions before embryos were dissected. E17.5 embryos and their placentas were weighed and inspected for any external morphological defects. Postnatal day 12 (P12) pups were sacrificed by carbon dioxide inhalation. FVB/N mice were purchased from Australian BioResources.

Mendelian ratios for all stages (E8.5, E15.5, E17.5, P12 and post-weaning) were analysed by chi-squared test. For statistical analysis of weights, embryo and placenta weights (E17.5) were normalised against the average weights of wildtype littermates. As embryo and placenta weight data did not follow a normal distribution, a Mann-Whitney (non-parametric) t-test was performed to determine statistical significance using Prism 8 (GraphPad). To compare mortality between heterozygous null and wildtype littermates in both strains (FVB/N and C57BL/6J) and all backcrosses, a two-tailed Fisher's exact test was used. To determine whether significantly more heterozygous null males die compared with heterozygous null females, a two-tailed Fisher's exact test was used.

Western Blotting

1.5×10^5 C2C12 cells were seeded on a 60 mm dish. After 24 hours, cells were transfected with 5 µg of either mouse *Wbp11* (untagged) or FLAG tagged mouse *Wbp11*. 24 hours post-transfection, cells were scraped and lysed in 50 µl WCE lysis buffer (20 mM HEPES pH 7.8, 420 mM NaCl, 0.5% NP40, 25% Glycerol, 0.2 mM EDTA, 1.5 mM $MgCl_2$, 1 mM PMSF, cOmplete protease inhibitor cocktail (Sigma)) and protein concentration was determined by bicinchononic acid (BCA) assay. To determine the endogenous expression levels of WBP11 in mammalian cells, a confluent 60 mm dish of C2C12 cells was lysed in 50 µl WCE. To determine endogenous WBP11 protein expression in embryos, proteins were extracted from a E9.5 wildtype embryo. The embryo was lysed in 30µl of RIPA buffer (20 mM Tris-HCl pH 7.5, 150 mM NaCl, 2 mM EDTA, 1% NP40, 1% Deoxycholate, 0.1% SDS,

UNCORRECTED MANUSCRIPT

Downloaded from https://academic.oup.com/hmg/advance-article/doi/10.1093/hmg/ddaa258/6020188 by Bodleian Law Library user on 07 December 2020

1 mM PMSF, cOmplete protease inhibitor cocktail (Sigma)). The supernatant was taken after a 15-minute spin at maximum speed (4°C) and stored at -80°C. Protein concentration was determined using BCA assay (50 μg of total protein was run on a 4-12% Bis-Tris gel). WBP11 expression was determined by Western blotting with WBP11 antibody (1:1000 PA5-31241; Pierce). β-Tubulin (1:5000; Sigma) was used as loading control.

Whole-mount immunofluorescence, histology and immunohistochemistry

Whole-mount immunofluorescence on E9.5 wildtype embryos was performed as described in (71) except that permeabilization was achieved by a 2-hour incubation in methanol: dimethyl sulfoxide (DMSO): 30% hydrogen peroxide (4:1:1) at room temperature and that embryos were blocked overnight in 10% donkey serum (Sigma D9663) dissolved in PBS containing 0.1% Triton X-100. Primary antibody for WBP11 (1:100) or Isotype control IgG and anti-rabbit RRX secondary antibody (1:100) was used. The embryos were cleared in BA:BB (benzyl alcohol: benzyl benzoate, Merck B6630) before imaging on an AxioObserver Z1 inverted microscope equipped with 710 scan head (Zeiss) using appropriate excitation/emission settings.

For paraffin sectioning, embryos (E10.5, E11.5 and E12.5) and kidneys of E17.5 embryos were fixed in 4% paraformaldehyde (PFA) overnight at 4°C, paraffin embedded and sectioned in the transverse plane (for whole mount embryos) and sagittal plane (for E17.5 kidneys) at 7 μm.

Immunohistochemistry was performed to determine the protein expression of WBP11 and Isotype IgG in mouse embryos. The paraffin-embedded tissue sections were deparaffinised and hydrated through xylene and graded ethanol series. Subsequently the sections were boiled in an antigen unmasking solution (10 mM Tris Base, 1 mM EDTA, 0.05% Tween20, pH9.0) and blocked for 1 hour in 10% donkey serum. For detection of

Downloaded from https://academic.oup.com/hmg/advance-article/doi/10.1093/hmg/ddaa258/6020188 by Bodleian Law Library user on 07 December 2020

UNCORRECTED MANUSCRIPT

WBP11 and Isotype IgG a horseradish peroxidase (HRP) donkey anti-rabbit secondary reagent and 3, 3' -diaminobenzidine (DAB) was used. After a Haematoxylin staining, sections were mounted with Gelvatol mounting media.

Histological sections of E17.5 kidneys were deparaffinised, stained with Haematoxylin (Sigma HHS16) and Eosin (Sigma Y E4382) and mounted in Depex before imaging on a Brightfield microscope (Leica MC170 HD).

Tomography

For assessment of the skeleton, FVB/N mouse pups were sacrificed at P12 and fixed in 4% PFA for 3 days before scanning. Micro-computed tomography (micro-CT) imaging of the entire skeletons was performed using the Skyscan 1272 scanner (Bruker) operated at 40 kV (source voltage), 238 µA (source current) and an Al 0.25mm filter. The magnification was set at 21.5 µm pixel size and images taken every 0.8º through 360º using 1216 ms exposure, generating 1497 projections in 30 minutes per field of view. Four fields of view were needed to capture the entire skeleton.

To assess soft tissues, E17.5 and E15.5 FVB/N embryos were dissected in cold 10 mM PBS (phosphate-buffered saline) and fixed in cold 4% PFA and 1% glutaraldehyde. Each embryo and their placenta were individually weighed and assessed for external morphological abnormalities. After 3 days, the embryos were immersed in hydrogel (4% acrylamide, 0.05% bis-acrylamide, 0.25% VA044 initiator and 0.05% saponin made up in PBS) (72) and incubated for an additional 3 days at 4 ºC with rocking. The hydrogel was polymerised at 37 ºC for 3 hours using an X-Clarity hydrogel embedding station (Logos) and subsequently removed to retrieve the stabilised embryo. Samples were immersed in 100% Lugol's solution (Sigma-Aldrich) for 5 days in the dark at room temperature and scanned using 75 kV source voltage, 238 µA source current, and an Al 0.5 mm + Cu 0.038 mm filter.

ACCEPTED MANUSCRIPT

Downloaded from https://academic.oup.com/hmg/advance-article/doi/10.1093/hmg/ddaa258/6020188 by Bodleian Law Library user on 07 December 2020

Magnification was set to 2.23 μm pixel resolution and images taken every 0.3º through 180º with an exposure of 2700 ms, generating 1923 projections in 1.5 hours for three fields of view. Acquired projections were reconstructed using NRecon software (Bruker) with smoothing, ring artefact and post-alignment corrections.

Analysis of micro-CT data, volume measurements and 3D rendering

To assess defects systematically, primary anatomical information was recorded for each embryo using CTvox (Bruker v3.3.0) with the aid of a checklist of 27 points covering cerebral, craniofacial, cardiac, gastrointestinal and limb defects for soft tissue analysis and 40 point for skeletal defects covering the skull, cervical, thoracic, lumbar and sacral regions. Morphological defects in affected organs were then quantified using Amira (Thermo Fisher). Rendering was performed in the segmentation editor of Amira by defining a global threshold to select only the skeleton. A surface view of this selection was then rendered. Reconstructed micro-CT datasets were also processed in the segmentation editor of Amira to obtain 3D volume measurements of the brain, kidneys, lungs and livers. To segment the organ of interest from the rest of the body, the brush tool was used to accurately select the appropriate pixels. Contours of the organ were selected manually using the brush tool every 10-20 slices, interpolated and then adjusted manually where necessary. Volume measurements of segmented organs were extracted from the material statistics table and normalised against the embryo weight. Statistical differences between genotypes were established with an unpaired t-test provided the dataset followed a normal distribution. If that was not the case, a non-parametric Mann-Whitney test was used.

UNCORRECTED MANUSCRIPT

Downloaded from https://academic.oup.com/hmg/advance-article/doi/10.1093/hmg/ddaa258/6020188 by Bodleian Law Library user on 07 December 2020

Accession Numbers

The *WBP11* variants described in this report have been submitted to ClinVar (SUB6661060).

Supplemental Data

Supplemental data include case reports, 6 figures and 4 tables and can be found with this article online at

Acknowledgments

The authors acknowledge the technical assistance of Melissa Rapadas, advice from Cedric Le Caignec and Vivette D'Agatti, and Matthew Brown for establishing the exome sequencing pipeline (for families 1 and 2). We also acknowledge Robert Brink and David Zahra of the Mouse Engineering at Garvan/Australian Bioresources (MEGA) service for their help in the design and generation of *Wbp11* CRISPR targeted allele. We gratefully acknowledge the assistance of the Marshfield Clinic, the Pediatrics Department of the University of Wisconsin-Madison, the Scoliosis Research Society and The Malika Ray, Asok K. Ray, M.D., FRCS/ (Edin) Initiative for Child Health Research. This work was supported by National Health and Medical Research Council (NHMRC) Project Grant ID1044543 to S.L.D, D.B.S. and E.L.D, Fellowships ID1135886, ID1042002 to S.L.D.; Office of Health and Medical Research NSW Government and The Victor Chang Cardiac Research Institute Innovation Centre, funded by the NSW Government; the Agence Nationale de la Recherche (CranioRespiro project and "Investissements d'avenir" program (ANR-10-IAHU-01)) and MSD Avenir (Devo-Decode project); and the National Institute of Health, National Institute of Diabetes and Digestive and Kidney Diseases Grant R01DK080099. Research reported in this publication was also supported in part by the Eunice Kennedy Shriver National Institute

UNCORRECTED MANUSCRIPT

Downloaded from https://academic.oup.com/hmg/advance-article/doi/10.1093/hmg/ddaa258/6020188 by Bodleian Law Library user on 07 December 2020

Of Child Health & Human Development of the National Institutes of Health under Award Number R03HD099516 to P.F.G and by the Baylor-Hopkins Center for Mendelian Genomics (NHGRI UM1 HG006542). We are grateful to the families for participating in this research.

Declaration of Interests

R.D.S has equity interest in and has received consulting fees from Acer Therapeutics and Censa Pharmaceuticals. He has received grant funding from Alexion, travel support from Pfizer, and consulting fees from Raptor, Biomarin, Alexion, E-Scape Bio, Health Advances, Precision for Value, and Best Doctors. He is an employee of PreventionGenetics. R.D.S has patents awarded but not licensed (no revenue) in the area of newborn screening for sterol and bile acid disorders.

Web Resources (if any)

OMIM, http://www.omim.org/

gnomAD, https://gnomad.broadinstitute.org/

UNCORRECTED MANUSCRIPT

Downloaded from https://academic.oup.com/hmg/advance-article/doi/10.1093/hmg/ddaa258/6020188 by Bodleian Law Library user on 07 December 2020

References

1 Christianson, A., Howson, C.P. and Modell, B. (2006) March of dimes, global report on birth defects. *March of Dimes*, .

2 Feldkamp, M.L., Carey, J.C., Byrne, J.L.B., Krikov, S. and Botto, L.D. (2017) Etiology and clinical presentation of birth defects: population based study. *B.M.J.*, **357**, j2249.

3 Low, K.J., Ansari, M., Jamra, R.A., Clarke, A., El Chehadeh, S., FitzPatrick, D.R., Greenslade, M., Henderson, A., Hurst, J., Keller, K. *et al.* (2017) PUF60 variants cause a syndrome of ID, short stature, microcephaly, coloboma, craniofacial, cardiac, renal and spinal features. *Eur. J. Hum. Genet.*, **25**, 552-559.

4 Vetro, A., Iascone, M., Limongelli, I., Ameziane, N., Gana, S., Della Mina, E., Giussani, U., Ciccone, R., Forlino, A., Pezzoli, L. *et al.* (2015) Loss-of-Function FANCL Mutations Associate with Severe Fanconi Anemia Overlapping the VACTERL Association. *Hum. Mutat.*, **36**, 562-568.

5 Savage, S.A., Ballew, B.J., Giri, N., Laboratory, N.D.C.G.R., Chandrasekharappa, S.C., Ameziane, N., de Winter, J., Alter, B.P. and Group, N.D.C.S.W. (2016) Novel FANCI mutations in Fanconi anemia with VACTERL association. *Am. J. Med. Genet. A.*, **170A**, 386-391.

6 Zweier, C., Albrecht, B., Mitulla, B., Behrens, R., Beese, M., Gillessen-Kaesbach, G., Rott, H.D. and Rauch, A. (2002) "Mowat-Wilson" syndrome with and without Hirschsprung disease is a distinct, recognizable multiple congenital anomalies-mental retardation syndrome caused by mutations in the zinc finger homeo box 1B gene. *Am. J. Med. Genet.*, **108**, 177-181.

UNCORRECTED MANUSCRIPT

Downloaded from https://academic.oup.com/hmg/advance-article/doi/10.1093/hmg/ddaa258/6020188 by Bodleian Law Library user on 07 December 2020

7 Kiefer, S.M., Ohlemiller, K.K., Yang, J., McDill, B.W., Kohlhase, J. and Rauchman, M. (2003) Expression of a truncated Sall1 transcriptional repressor is responsible for Townes-Brocks syndrome birth defects. *Hum. Mol. Genet.*, **12**, 2221-2227.

8 Shi, H., Enriquez, A., Rapadas, M., Martin, E., Wang, R., Moreau, J., Lim, C.K., Szot, J.O., Ip, E., Hughes, J.N. *et al.* (2017) NAD Deficiency, Congenital Malformations, and Niacin Supplementation. *N. Engl. J. Med.*, **377**, 544-552.

9 Szot, J.O., Campagnolo, C., Cao, Y., Iyer, K.R., Cuny, H., Drysdale, T., Flores-Daboub, J.A., Bi, W., Westerfield, L., Liu, P. *et al.* (2020) Bi-allelic Mutations in NADSYN1 Cause Multiple Organ Defects and Expand the Genotypic Spectrum of Congenital NAD Deficiency Disorders. *Am. J. Hum. Genet.*, **106**, 129-136.

10 Husain, M., Dutra-Clarke, M., Lemieux, B., Wencel, M., Solomon, B.D. and Kimonis, V. (2018) Phenotypic diversity of patients diagnosed with VACTERL association. *Am. J. Med. Genet. A.*, **176**, 1830-1837.

11 Solomon, B.D., Pineda-Alvarez, D.E., Raam, M.S. and Cummings, D.A. (2010) Evidence for inheritance in patients with VACTERL association. *Hum. Genet.*, **127**, 731-733.

12 Solomon, B.D. (2018) The etiology of VACTERL association: Current knowledge and hypotheses. *Am. J. Med. Genet. C. Semin. Med. Genet.*, **178**, 440-446.

13 Bartels, E., Jenetzky, E., Solomon, B.D., Ludwig, M., Schmiedeke, E., Grasshoff-Derr, S., Schmidt, D., Marzheuser, S., Hosie, S., Weih, S. *et al.* (2012) Inheritance of the VATER/VACTERL association. *Pediatr. Surg. Int.*, **28**, 681-685.

14 Craggs, G., Finan, P.M., Lawson, D., Wingfield, J., Perera, T., Gadher, S., Totty, N.F. and Kellie, S. (2001) A Nuclear SH3 Domain-binding Protein That Colocalizes with mRNA Splicing Factors and Intermediate Filament-containing Perinuclear Networks. *J. Biol. Chem.*, **276**, 30552-30560.

UNCORRECTED MANUSCRIPT

Downloaded from https://academic.oup.com/hmg/advance-article/doi/10.1093/hmg/ddaa258/6020188 by Bodleian Law Library user on 07 December 2020

15 Galganski, L., Urbanek, M.O. and Krzyzosiak, W.J. (2017) Nuclear speckles: molecular organization, biological function and role in disease. *Nucleic Acids Res.*, **45**, 10350-10368.

16 Deckert, J., Hartmuth, K., Boehringer, D., Behzadnia, N., Will, C.L., Kastner, B., Stark, H., Urlaub, H. and Lührmann, R. (2006) Protein Composition and Electron Microscopy Structure of Affinity-Purified Human Spliceosomal B Complexes Isolated under Physiological Conditions. *Mol. Cell. Biol.*, **26**, 5528-5543.

17 Agafonov, D.E., Deckert, J., Wolf, E., Odenwalder, P., Bessonov, S., Will, C.L., Urlaub, H. and Luhrmann, R. (2011) Semiquantitative proteomic analysis of the human spliceosome via a novel two-dimensional gel electrophoresis method. *Mol. Cell Biol.*, **31**, 2667-2682.

18 Fredericks, A.M., Cygan, K.J., Brown, B.A. and Fairbrother, W.G. (2015) RNA-Binding Proteins: Splicing Factors and Disease. *Biomolecules*, **5**, 893-909.

19 Sobreira, N., Schiettecatte, F., Valle, D. and Hamosh, A. (2015) GeneMatcher: a matching tool for connecting investigators with an interest in the same gene. *Hum. Mutat.*, **36**, 928-930.

20 Kurosaki, T. and Maquat, L.E. (2016) Nonsense-mediated mRNA decay in humans at a glance. *J. Cell Sci.*, **129**, 461-467.

21 Karczewski, K.J., Francioli, L.C., Tiao, G., Cummings, B.B., Alfoldi, J., Wang, Q., Collins, R.L., Laricchia, K.M., Ganna, A., Birnbaum, D.P. *et al.* (2020) The mutational constraint spectrum quantified from variation in 141,456 humans. *Nature*, **581**, 434-443.

22 Jaganathan, K., Kyriazopoulou Panagiotopoulou, S., McRae, J.F., Darbandi, S.F., Knowles, D., Li, Y.I., Kosmicki, J.A., Arbelaez, J., Cui, W., Schwartz, G.B. *et al.* (2019) Predicting Splicing from Primary Sequence with Deep Learning. *Cell*, **176**, 535-548 e524.

UNCORRECTED MANUSCRIPT

Downloaded from https://academic.oup.com/hmg/advance-article/doi/10.1093/hmg/ddaa258/6020188 by Bodleian Law Library user on 07 December 2020

23 Monger, S., Troup, M., Ip, E., Dunwoodie, S.L. and Giannoulatou, E. (2019) Spliceogen: An integrative, scalable tool for the discovery of splice-altering variants. *Bioinfo.*, **35**, 4405-4407.

24 Yeo, G. and Burge, C.B. (2004) Maximum entropy modeling of short sequence motifs with applications to RNA splicing signals. *J. Comput. Biol.*, **11**, 377-394.

25 Al Dhaheri, N., Wu, N., Zhao, S., Wu, Z., Blank, R.D., Zhang, J., Raggio, C., Halanski, M., Shen, J., Noonan, K. *et al.* (2020) KIAA1217: A novel candidate gene associated with isolated and syndromic vertebral malformations. *Am. J. Med. Genet. A.*, **182**, 1664-1672.

26 Bernier, R., Steinman, K.J., Reilly, B., Wallace, A.S., Sherr, E.H., Pojman, N., Mefford, H.C., Gerdts, J., Earl, R., Hanson, E. *et al.* (2016) Clinical phenotype of the recurrent 1q21.1 copy-number variant. *Genet. Med.*, **18**, 341-349.

27 Lee, S., Emond, M.J., Bamshad, M.J., Barnes, K.C., Rieder, M.J., Nickerson, D.A., Team, N.G.E.S.P.-E.L.P., Christiani, D.C., Wurfel, M.M. and Lin, X. (2012) Optimal unified approach for rare-variant association testing with application to small-sample case-control whole-exome sequencing studies. *Am. J. Hum. Genet.*, **91**, 224-237.

28 Hsu, C.W., Wong, L., Rasmussen, T.L., Kalaga, S., McElwee, M.L., Keith, L.C., Bohat, R., Seavitt, J.R., Beaudet, A.L. and Dickinson, M.E. (2016) Three-dimensional microCT imaging of mouse development from early post-implantation to early postnatal stages. *Dev. Biol.*, **419**, 229-236.

29 Yang, D.W., Xie, Z.Y., Stephenson, D., Morton, D., Hicks, C.D., Brown, T.M., Sriram, R., O'Neill, S., Raunig, D. and Bocan, T. (2011) Volumetric MRI and MRS provide sensitive measures of Alzheimer's disease neuropathology in inducible Tau transgenic mice (rTg4510). *Neuroimage*, **54**, 2652-2658.

UNCORRECTED MANUSCRIPT

Downloaded from https://academic.oup.com/hmg/advance-article/doi/10.1093/hmg/ddaa258/6020188 by Bodleian Law Library user on 07 December 2020

30 Harrison, S.J., Nishinakamura, R., Jones, K.R. and Monaghan, A.P. (2012) Sall1 regulates cortical neurogenesis and laminar fate specification in mice: implications for neural abnormalities in Townes-Brocks syndrome. *Dis. Model Mech.*, **5**, 351-365.

31 Bedford, M.T., Reed, R. and Leder, P. (1998) WW domain-mediated interactions reveal a spliceosome-associated protein that binds a third class of proline-rich motif: the proline glycine and methionine-rich motif. *Proc. Natl. Acad. Sci. USA*, **95**, 10602-10607.

32 Llorian, M., Beullens, M., Andrés, I., Ortiz, J.-M. and Bollen, M. (2004) SIPP1, a novel pre-mRNA splicing factor and interactor of protein phosphatase-1. *Biochem. J.*, **378**, 229-238.

33 Llorian, M., Beullens, M., Lesage, B., Nicolaescu, E., Beke, L., Landuyt, W., Ortiz, J.-M. and Bollen, M. (2005) Nucleocytoplasmic shuttling of the splicing factor SIPP1. *J. Biol. Chem.*, **280**, 38862-38869.

34 Lek, M., Karczewski, K.J., Minikel, E.V., Samocha, K.E., Banks, E., Fennell, T., O'Donnell-Luria, A.H., Ware, J.S., Hill, A.J., Cummings, B.B. *et al.* (2016) Analysis of protein-coding genetic variation in 60,706 humans. *Nature*, **536**, 285-291.

35 Abou Tayoun, A.N., Pesaran, T., DiStefano, M.T., Oza, A., Rehm, H.L., Biesecker, L.G., Harrison, S.M. and ClinGen Sequence Variant Interpretation Working, G. (2018) Recommendations for interpreting the loss of function PVS1 ACMG/AMP variant criterion. *Hum. Mutat.*, **39**, 1517-1524.

36 Richards, S., Aziz, N., Bale, S., Bick, D., Das, S., Gastier-Foster, J., Grody, W.W., Hegde, M., Lyon, E., Spector, E. *et al.* (2015) Standards and guidelines for the interpretation of sequence variants: a joint consensus recommendation of the American College of Medical Genetics and Genomics and the Association for Molecular Pathology. *Genet. Med.*, **17**, 405-423.

UNCORRECTED MANUSCRIPT

Downloaded from https://academic.oup.com/hmg/advance-article/doi/10.1093/hmg/ddaa258/6020188 by Bodleian Law Library user on 07 December 2020

37 Stevenson, R.E., Bennett, C.W., Abidi, F., Kleefstra, T., Porteous, M., Simensen, R.J., Lubs, H.A., Hamel, B.C.J. and Schwartz, C.E. (2005) Renpenning syndrome comes into focus. *Am. J. Med. Genet. A*, **134A**, 415-421.

38 Germanaud, D., Rossi, M., Bussy, G., Gérard, D., Hertz-Pannier, L., Blanchet, P., Dollfus, H., Giuliano, F., Bennouna-Greene, V., Sarda, P. *et al.* (2010) The Renpenning syndrome spectrum: new clinical insights supported by 13 new PQBP1-mutated males. *Clin. Genet.*, **79**, 225-235.

39 Wang, Q., Moore, M.J., Adelmant, G., Marto, J.A. and Silver, P.A. (2013) PQBP1, a factor linked to intellectual disability, affects alternative splicing associated with neurite outgrowth. *Genes Dev.*, **27**, 615-626.

40 Yoh, S.M., Schneider, M., Seifried, J., Soonthornvacharin, S., Akleh, R.E., Olivieri, K.C., De Jesus, P.D., Ruan, C., de Castro, E., Ruiz, P.A. *et al.* (2015) PQBP1 Is a Proximal Sensor of the cGAS-Dependent Innate Response to HIV-1. *Cell*, **161**, 1293-1305.

41 Okazawa, H. (2018) PQBP1, an intrinsically disordered/denatured protein at the crossroad of intellectual disability and neurodegenerative diseases. *Neurochem. Int.*, **119**, 17-25.

42 Lubs, H., Abidi, F.E., Echeverri, R., Holloway, L., Meindl, A., Stevenson, R.E. and Schwartz, C.E. (2006) Golabi-Ito-Hall syndrome results from a missense mutation in the WW domain of the PQBP1 gene. *J. Med. Genet.*, **43**, e30.

43 Tapia, V.E., Nicolaescu, E., McDonald, C.B., Musi, V., Oka, T., Inayoshi, Y., Satteson, A.C., Mazack, V., Humbert, J., Gaffney, C.J. *et al.* (2010) Y65C Missense Mutation in the WW Domain of the Golabi-Ito-Hall Syndrome Protein PQBP1 Affects Its Binding Activity and Deregulates Pre-mRNA Splicing. *J. Biol. Chem.*, **285**, 19391-19401.

44 Iwasaki, Y. and Thomsen, G.H. (2014) The splicing factor PQBP1 regulates mesodermal and neural development through FGF signaling. *Dev.*, **141**, 3740-3751.

UNCORRECTED MANUSCRIPT

Downloaded from https://academic.oup.com/hmg/advance-article/doi/10.1093/hmg/ddaa258/6020188 by Bodleian Law Library user on 07 December 2020

45 Wieczorek, D., Newman, W.G., Wieland, T., Berulava, T., Kaffe, M., Falkenstein, D., Beetz, C., Graf, E., Schwarzmayr, T., Douzgou, S. *et al.* (2014) Compound Heterozygosity of Low-Frequency Promoter Deletions and Rare Loss-of-Function Mutations in TXNL4A Causes Burn-McKeown Syndrome. *Am. J. Hum. Genet.*, **95**, 698-707.

46 Tooley, M., Lynch, D., Bernier, F., Parboosingh, J., Bhoj, E., Zackai, E., Calder, A., Itasaki, N., Wakeling, E., Scott, R. *et al.* (2016) Cerebro-costo-mandibular syndrome: Clinical, radiological, and genetic findings. *Am. J. Med. Genet. A.*, **170A**, 1115-1126.

47 Lynch, D.C., Revil, T., Schwartzentruber, J., Bhoj, E.J., Innes, A.M., Lamont, R.E., Lemire, E.G., Chodirker, B.N., Taylor, J.P., Zackai, E.H. *et al.* (2014) Disrupted auto-regulation of the spliceosomal gene SNRPB causes cerebro-costo-mandibular syndrome. *Nat. Commun.*, **5**, 4483.

48 El Chehadeh, S., Kerstjens-Frederikse, W.S., Thevenon, J., Kuentz, P., Bruel, A.-L., Thauvin-Robinet, C., Bensignor, C., Dollfus, H., Laugel, V., Rivière, J.-B. *et al.* (2017) Dominant variants in the splicing factor PUF60 cause a recognizable syndrome with intellectual disability, heart defects and short stature. *Eur. J. Hum. Genet.*, **25**, 43-51.

49 Au, P.Y.B., You, J., Caluseriu, O., Schwartzentruber, J., Majewski, J., Bernier, F.P., Ferguson, M., Care for Rare Canada, C., Valle, D., Parboosingh, J.S. *et al.* (2015) GeneMatcher aids in the identification of a new malformation syndrome with intellectual disability, unique facial dysmorphisms, and skeletal and connective tissue abnormalities caused by de novo variants in HNRNPK. *Hum. Mutat.*, **36**, 1009-1014.

50 Yang, J., Zhao, Y., Kalita, M., Li, X., Jamaluddin, M., Tian, B., Edeh, C.B., Wiktorowicz, J.E., Kudlicki, A. and Brasier, A.R. (2015) Systematic Determination of Human Cyclin Dependent Kinase (CDK)-9 Interactome Identifies Novel Functions in RNA Splicing Mediated by the DEAD Box (DDX)-5/17 RNA Helicases. *Mol. Cell Prot.*, **14**, 2701-2721.

UNCORRECTED MANUSCRIPT

Downloaded from https://academic.oup.com/hmg/advance-article/doi/10.1093/hmg/ddaa258/6020188 by Bodleian Law Library user on 07 December 2020

51 Shaheen, R., Patel, N., Shamseldin, H., Alzahrani, F., Al-Yamany, R., A, A.L., Ewida, N., Anazi, S., Alnemer, M., Elsheikh, M. *et al.* (2016) Accelerating matchmaking of novel dysmorphology syndromes through clinical and genomic characterization of a large cohort. *Genet. Med.*, **18**, 686-695.

52 Malinová, A., Cvačková, Z., Matějů, D., Hořejší, Z., Abéza, C., Vandermoere, F., Bertrand, E., Staněk, D. and Verheggen, C. (2017) Assembly of the U5 snRNP component PRPF8 is controlled by the HSP90/R2TP chaperones. *J. Cell Biol.*, **216**, 1579-1596.

53 Lines, M.A., Huang, L., Schwartzentruber, J., Douglas, S.L., Lynch, D.C., Beaulieu, C., Guion-Almeida, M.L., Zechi-Ceide, R.M., Gener, B., Gillessen Kaesbach, G. *et al.* (2012) Haploinsufficiency of a Spliceosomal GTPase Encoded by EFTUD2 Causes Mandibulofacial Dysostosis with Microcephaly. *Am. J. Hum. Genet.*, **90**, 369-377.

54 Gordon, C.T., Petit, F., Oufadem, M., Decaestecker, C., Jourdain, A.-S., Andrieux, J., Malan, V., Alessandri, J.-L., Baujat, G., Baumann, C. *et al.* (2012) EFTUD2 haploinsufficiency leads to syndromic oesophageal atresia. *J. Med. Genet.*, **49**, 737-746.

55 Kim, J.-H., Shinde, D.N., Reijnders, M.R.F., Hauser, N.S., Belmonte, R.L., Wilson, G.R., Bosch, D.G.M., Bubulya, P.A., Shashi, V., Petrovski, S. *et al.* (2016) De Novo Mutations in SON Disrupt RNA Splicing of Genes Essential for Brain Development and Metabolism, Causing an Intellectual-Disability Syndrome. *Am. J. Hum. Genet.*, **99**, 711-719.

56 Tokita, M.J., Braxton, A.A., Shao, Y., Lewis, A.M., Vincent, M., Küry, S., Besnard, T., Isidor, B., Latypova, X., Bézieau, S. *et al.* (2016) De Novo Truncating Variants in SON Cause Intellectual Disability, Congenital Malformations, and Failure to Thrive. *Am. J. Hum. Genet.*, **99**, 720-727.

57 Xu, M., Xie, Y.A., Abouzeid, H., Gordon, C.T., Fiorentino, A., Sun, Z., Lehman, A., Osman, I.S., Dharmat, R., Riveiro-Alvarez, R. *et al.* (2017) Mutations in the Spliceosome

UNCORRECTED MANUSCRIPT

Downloaded from https://academic.oup.com/hmg/advance-article/doi/10.1093/hmg/ddaa258/6020188 by Bodleian Law Library user on 07 December 2020

Component CWC27 Cause Retinal Degeneration with or without Additional Developmental Anomalies. *Am. J. Hum. Genet.*, **100**, 592-604.

58 Ghebranious, N., Blank, R.D., Raggio, C.L., Staubli, J., McPherson, E., Ivacic, L., Rasmussen, K., Jacobsen, F.S., Faciszewski, T., Burmester, J.K. *et al.* (2008) A missense T (Brachyury) mutation contributes to vertebral malformations. *J. Bone Miner. Res.*, **23**, 1576-1583.

59 Wu, N., Ming, X., Xiao, J., Wu, Z., Chen, X., Shinawi, M., Shen, Y., Yu, G., Liu, J., Xie, H. *et al.* (2015) TBX6 null variants and a common hypomorphic allele in congenital scoliosis. *N. Engl. J. Med.*, **372**, 341-350.

60 Edwards, J.J. and Gelb, B.D. (2016) Genetics of congenital heart disease. *Curr. Opin. Cardiol.*, **31**, 235-241.

61 Sparrow, D.B., Chapman, G., Smith, A.J., Mattar, M.Z., Major, J.A., O'Reilly, V.C., Saga, Y., Zackai, E.H., Dormans, J.P., Alman, B.A. *et al.* (2012) A mechanism for gene-environment interaction in the etiology of congenital scoliosis. *Cell*, **149**, 295-306.

62 Van de Putte, R., De Walle, H.E., Van Hooijdonk, K.J., De Blaauw, I., Marcelis, C.L., van Heijst, A., Giltay, J.C., Renkema, K.Y., Broens, P.M. and Brosens, E.J.B.D.R. (2020) Maternal risk associated with the VACTERL association: A case–control study. *Birth Defects Res.*, **1-10**.

63 Hilger, A., Schramm, C., Draaken, M., Mughal, S.S., Dworschak, G., Bartels, E., Hoffmann, P., Nothen, M.M., Reutter, H. and Ludwig, M. (2012) Familial occurrence of the VATER/VACTERL association. *Pediatr. Surg. Int.*, **28**, 725-729.

64 Meehan, T.F., Conte, N., West, D.B., Jacobsen, J.O., Mason, J., Warren, J., Chen, C.K., Tudose, I., Relac, M., Matthews, P. *et al.* (2017) Disease model discovery from 3,328 gene knockouts by The International Mouse Phenotyping Consortium. *Nat. Genet.*, **49**, 1231-1238.

UNCORRECTED MANUSCRIPT

Downloaded from https://academic.oup.com/hmg/advance-article/doi/10.1093/hmg/ddaa258/6020188 by Bodleian Law Library user on 07 December 2020

65 Sittig, L.J., Carbonetto, P., Engel, K.A., Krauss, K.S., Barrios-Camacho, C.M. and Palmer, A.A. (2016) Genetic Background Limits Generalizability of Genotype-Phenotype Relationships. *Neuron*, **91**, 1253-1259.

66 Passemard, S., Kaindl, A.M. and Verloes, A. (2013) *Microcephaly*. Elsevier B.V.

67 Ito, H., Shiwaku, H., Yoshida, C., Homma, H., Luo, H., Chen, X., Fujita, K., Musante, L., Fischer, U., Frints, S.G.M. *et al.* (2015) In utero gene therapy rescues microcephaly caused by Pqbp1-hypofunction in neural stem progenitor cells. *Mol. Psychiatry*, **20**, 459-471.

68 Dawes, R., Lek, M. and Cooper, S.T. (2019) Gene discovery informatics toolkit defines candidate genes for unexplained infertility and prenatal or infantile mortality. *NPJ Genom. Med.*, **4**, 8.

69 Chapman, G., Moreau, J.L.M., I, P.E., Szot, J.O., Iyer, K.R., Shi, H., Yam, M.X., O'Reilly, V.C., Enriquez, A., Greasby, J.A. *et al.* (2020) Functional genomics and gene-environment interaction highlight the complexity of congenital heart disease caused by Notch pathway variants. *Hum. Mol. Genet.*, **29**, 566-579.

70 Brayton, C. (2013) Spontaneous diseases in commonly used mouse strains / stocks. *The mouse in Biomedical Research*, **2**.

71 Geffers, I., Serth, K., Chapman, G., Jaekel, R., Schuster-Gossler, K., Cordes, R., Sparrow, D.B., Kremmer, E., Dunwoodie, S.L., Klein, T. *et al.* (2007) Divergent functions and distinct localization of the Notch ligands DLL1 and DLL3 in vivo. *J. Cell Biol.*, **178**, 465-476.

72 Wong, M.D., Spring, S. and Henkelman, R.M. (2013) Structural Stabilization of Tissue for Embryo Phenotyping Using Micro-CT with Iodine Staining. *PLoS ONE*, **8**, e84321.

UNCORRECTED MANUSCRIPT

Downloaded from https://academic.oup.com/hmg/advance-article/doi/10.1093/hmg/ddaa258/6020188 by Bodleian Law Library user on 07 December 2020

Figure legends

Figure 1. *WBP11* variants and vertebral segmentation defects in selected individuals.

(A) Schematic representation of the *WBP11* open reading frame and cDNA (bottom) with variants and protein structure (top). PRR, Proline rich region. (B) Patient 1A has C3-C4 (arrowhead), C6-C7 fusion/block vertebrae (not shown) and bilateral omovertebral bones from C5 (asterisk). (C) Patient 1B has T12 butterfly vertebrae (arrowhead) and congenital scoliosis. Patient 2 has C6-C7 fusion (D, arrowhead) and T2 left hemifusion (E, asterisk) and T1, T4 butterfly vertebrae (E, arrowheads).

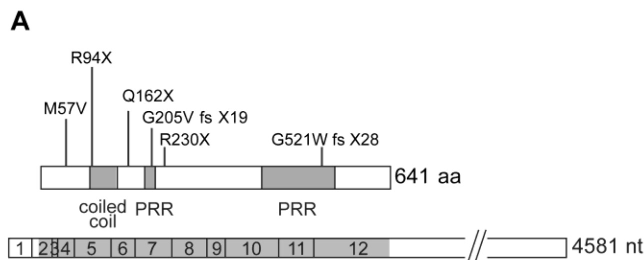

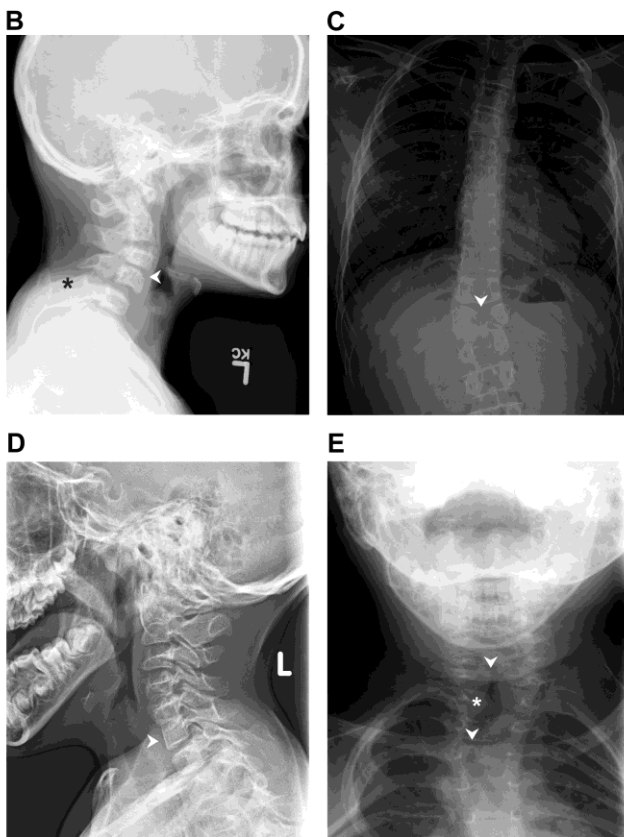

ACCEPTED MANUSCRIPT

Downloaded from https://academic.oup.com/hmg/advance-article/doi/10.1093/hmg/ddaa258/6020188 by Bodleian Law Library user on 07 December 2020

Figure 2. *Wbp11*$^{-/-}$ and *Wbp11*$^{+/-}$ embryos and mice do not survive in expected numbers.

(A) Number of *Wbp11*$^{+/-}$ and *Wbp11*$^{+/+}$ mice observed compared with the expected Mendelian ratio (dotted line) at E17.5 (backcross 2,* $p = 0.0263$), P12 (backcross 2 , * $p = 0.0412$), and post-weaning (backcrosses 1 and 2, **** $p = 0.0001$). Deviation from expected Mendelian ratios for the *Wbp11*$^{+/-}$ × *Wbp11*$^{+/+}$ breeding scheme was calculated by chi-squared test. Dead mice that could not be genotyped were omitted. (B) Percentage of male and female *Wbp11*$^{+/-}$ mice that died postnatally. On the left, FVB/N background backcrosses 1 to 4, ** $p = 0.0063$. On the right, C57BL/6J background crosses 1 to 4, ** $p = 0.0049$. Fisher's exact test was used to determine significance. (C) Comparison of *Wbp11*$^{+/+}$ and *Wbp11*$^{+/-}$ embryo weights at E17.5 normalised to average wildtype body weight (n = 98, **** p <0.0001). (D) Photomicrographs and contrast-enhanced micro-CT scans of E17.5 embryos illustrating the smaller size of *Wbp11*$^{+/-}$ embryos and the presence of oedema (arrowhead) compared with wildtype embryos from the same litter. (E) Placenta weight of E17.5 embryos (FVB/N) after dissection, normalised to average wildtype placenta weight (n = 98, * $p = 0.0239$). (F) *Wbp11*$^{+/-}$ and *Wbp11*$^{+/+}$ E17.5 embryo weights normalised to the weights of their placentas (**** p <0.0001). (G) Embryo genotypes observed at E8.5 in litters from *Wbp11*$^{+/-}$ × *Wbp11*$^{+/-}$ matings (backcrosses 2 and 3). Deviation from expected Mendelian ratios (dotted lines) was calculated by chi-squared test ($p = 0.0007$). (H) Photomicrographs of *Wbp11*$^{+/-}$ and wildtype E8.5 embryos. Error bars represent SD. (C, E and F) Unpaired t-test was used to determine significance and red dots indicate the embryos in D. Scale bars: 5 mm (D), 500 µm (H) .

Downloaded from https://academic.oup.com/hmg/advance-article/doi/10.1093/hmg/ddaa258/6020188 by Bodleian Law Library user on 07 December 2020

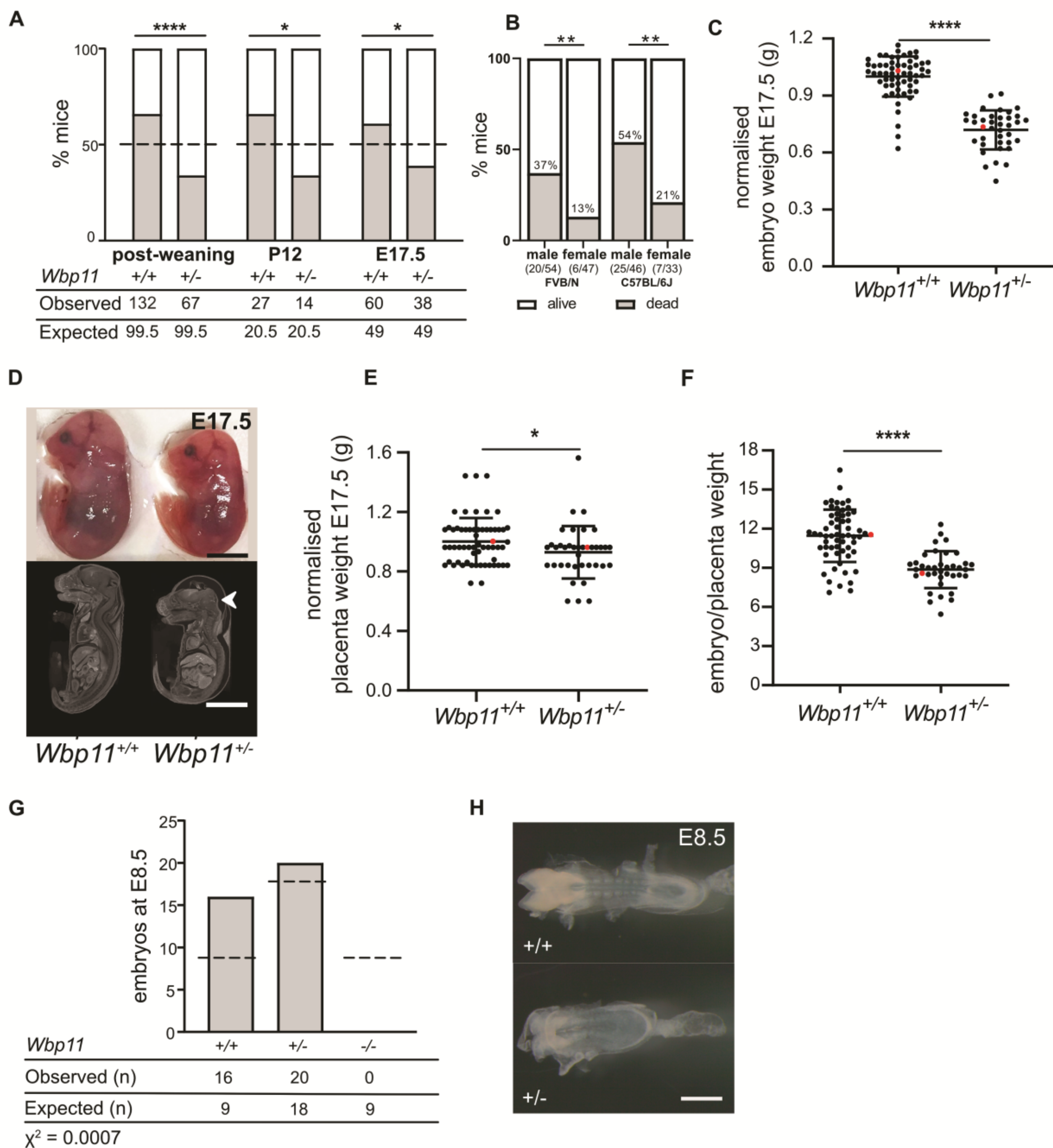

UNCORRECTED MANUSCRIPT

Downloaded from https://academic.oup.com/hmg/advance-article/doi/10.1093/hmg/ddaa258/6020188 by Bodleian Law Library user on 07 December 2020

Figure 3. *Wbp11*$^{+/-}$ mice exhibit axial skeletal defects.

Surface views of micro-CT reconstructions illustrating skeletal defects in *Wbp11*$^{+/-}$ (right) compared with wildtype P12 pups (left). Pups included in this data are from the 2nd backcross. (A) Anterior and (B) posterior halves of the cervical vertebrae of a *Wbp11*$^{+/-}$ (right) and a wildtype P12 pup (left). The atlas (C1) has been removed to allow visualisation of defects in the axis (C2). In this *Wbp11*$^{+/-}$ pup, the axis and C4 are missing vertebral bodies, the anterior arches of the axis are fused to C3, the right anterior arch of C4 is fused to C3 and C5 (A), and the midline of the neural arches (B) is asymmetrical. (C) Anterior portion of the thoracic cage showing fusion of sternebrae 3 and 4, common in *Wbp11*$^{+/-}$ mice. In this example, a true rib is missing from the right side (arrowhead) of the mouse. (D) Anterior view of the thorax of a *Wbp11*$^{+/-}$ mouse with a vertebral fusion (T10-T11 fusion). (E) Anterior view of the lumbar vertebrae. Scale bars: 2 mm.

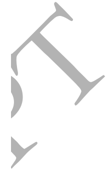

UNCORRECTED MANUSCRIPT

Downloaded from https://academic.oup.com/hmg/advance-article/doi/10.1093/hmg/ddaa258/6020188 by Bodleian Law Library user on 07 December 2020

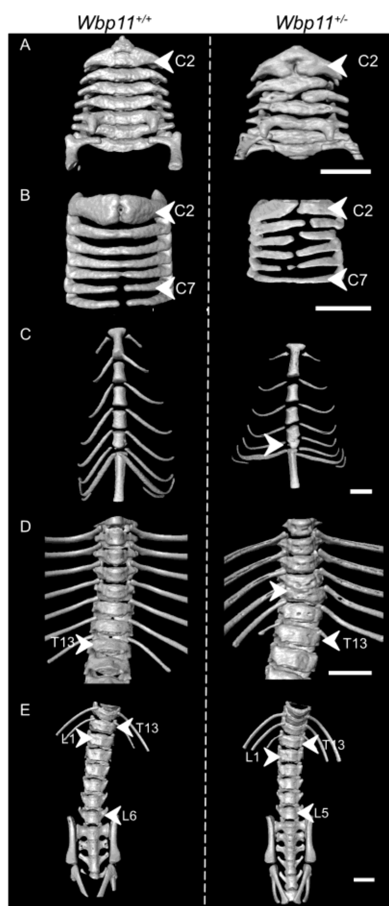

UNCORRECTED MANUSCRIPT

Downloaded from https://academic.oup.com/hmg/advance-article/doi/10.1093/hmg/ddaa258/6020188 by Bodleian Law Library user on 07 December 2020

Figure 4. Brains of *Wbp11*$^{+/-}$ embryos are smaller than *Wbp11*$^{+/+}$ littermates.

(A) Head of *Wbp11*$^{+/+}$ (top) and *Wbp11*$^{+/-}$ (bottom) E17.5 embryos in sagittal section of contrast-enhanced micro-CT scans. (B) Quantification of the total brain volume normalised to each embryo's weight (p <0.0001). (C) Schematic diagram of measurements taken from the brains (E17.5). AP length is the maximum length in the anteroposterior axis of the brain. Cortical width is the maximum cross brain distance at the level of lateral ventricle and third ventricle while cortical thickness is measured at the level of the third ventricle. (D-F) Comparison of *Wbp11*$^{+/+}$ to *Wbp11*$^{+/-}$ measurements of the brain including AP length (D, ** p = 0.004), cortical width (E, **** p <0.0001) and cortical thickness (F, **** p <0.0001). Embryos included in this data are from the 2nd backcross. Unpaired t-test was used to determine statistical significance. Error bars represent SD. Open dots indicate the embryos in A. Scale bar: 2 mm (A).

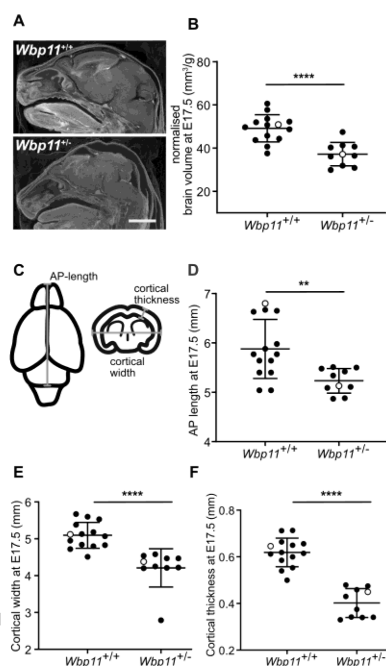

ACCEPTED MANUSCRIPT

Downloaded from https://academic.oup.com/hmg/advance-article/doi/10.1093/hmg/ddaa258/6020188 by Bodleian Law Library user on 07 December 2020

Figure 5. Kidney defects are present in E17.5 *Wbp11*$^{+/-}$ embryos.

(A) Anterior view of micro-CT reconstructions comparing kidney morphology between *Wbp11*$^{+/+}$ and *Wbp11*$^{+/-}$ littermates at E17.5. Left kidney is indicated. Graph shows comparison of volume measurements of left and right kidneys in *Wbp11*$^{+/+}$ and *Wbp11*$^{+/-}$ littermates at E17.5 (left kidney, ** $p = 0.0024$; right kidney, *** $p = 0.0002$). Red dots indicate the embryos on the left. (B) Histological sections (sagittal) stained with haematoxylin and eosin of an E17.5 kidney from *Wbp11*$^{+/+}$ (top 2 panels) and *Wbp11*$^{+/-}$ embryos (bottom 2 panels). Whole kidney micrographs (left) and high magnifications (right) are shown. (C) 3D surface view of the lungs combined with micro-CT reconstruction slice (anterior view). Volume measurements of the lungs from *Wbp11*$^{+/+}$ and *Wbp11*$^{+/-}$ littermates at E17.5 (** $p = 0.0034$). Red dots indicate embryos on the left. (D) 3D surface view of the liver combined with micro-CT reconstruction slice (anterior view). Volume measurements of the livers from *Wbp11*$^{+/+}$ and *Wbp11*$^{+/-}$ littermates at E17.5 (*** $p = 0.0001$). Red dots indicate embryos on the left. Embryos included in this data are from the 2nd backcross. Kidney, lung and liver volumes were normalised against embryo weight. Unpaired t-test was performed to determine statistical significance. Scale bars: 2 mm (A), whole kidney = 500 μm and high magnification = 100 μm (B), 5 mm (C, D). Error bars represent SD.

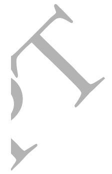

UNCO

Downloaded from https://academic.oup.com/hmg/advance-article/doi/10.1093/hmg/ddaa258/6020188 by Bodleian Law Library user on 07 December 2020

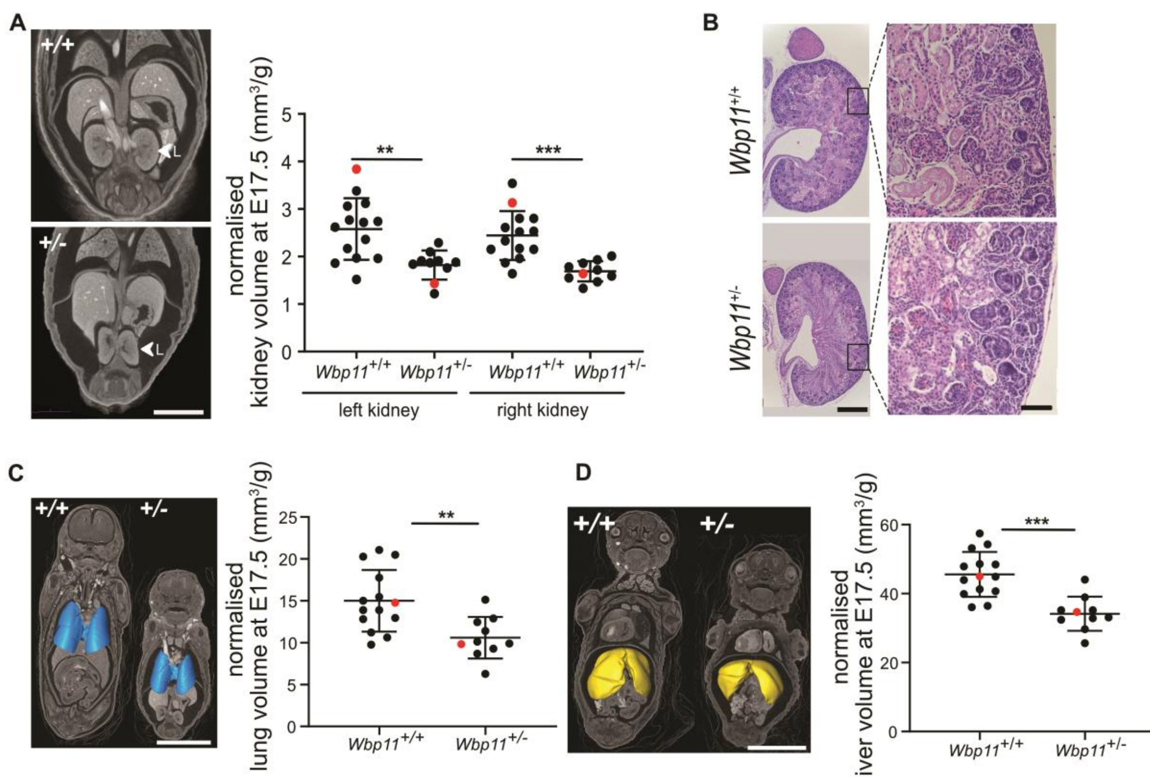

UNCORRECTED MANUSCRIPT

Downloaded from https://academic.oup.com/hmg/advance-article/doi/10.1093/hmg/ddaa258/6020188 by Bodleian Law Library user on 07 December 2020

Figure 6. WBP11 is ubiquitously expressed in mouse embryos.

(A) Immunoblot showing WBP11 (lane 1) and WBP11-FLAG (lane 2) over-expression in C2C12 mouse cell line and endogenous WBP11 expression in C2C12 (lane 3) and E9.5 embryo lysate (lane 4). Beta-tubulin was used as a loading control. (B) Whole-mount immunofluorescence staining of an E9.5 mouse embryo with anti-WBP11 antibody. Anti-WBP11 reactivity was detected with donkey anti-rabbit RRX. (C-K) Transverse sections of paraffin embedded mouse embryos at different stages labelled with anti-WBP11 antibody (left 2 columns) or IgG isotype control (right column) followed by detection with anti-rabbit HRP and DAB staining. (C-E) Sections through the neural tube at E10.5. (F-H) Sections through the kidney at E12.5. (I-K) Sections through the heart at E12.5. All paraffin sections were counterstained with Hematoxylin, dorsal is to the top and ventral to the bottom. s: somite nt: neural tube, cc: central canal, cm: condensed mesenchyme, ub: uretric bud, rv: right ventricle, lv: left ventricle, ra: right atrium, la: left atrium. Scale bars: 500 µm (I, K), 300 µm (C, E, F, H), 100 µm (B, D, G, J).

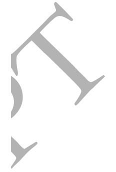

UNCORRECTED MANUSCRIPT

Downloaded from https://academic.oup.com/hmg/advance-article/doi/10.1093/hmg/ddaa258/6020188 by Bodleian Law Library user on 07 December 2020

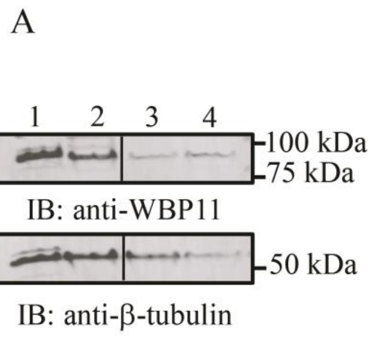

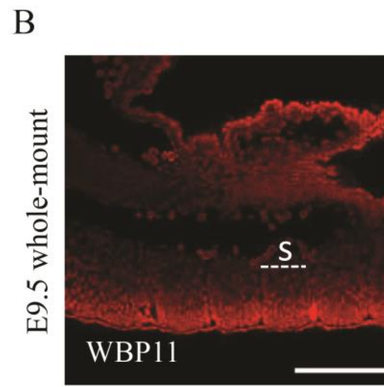

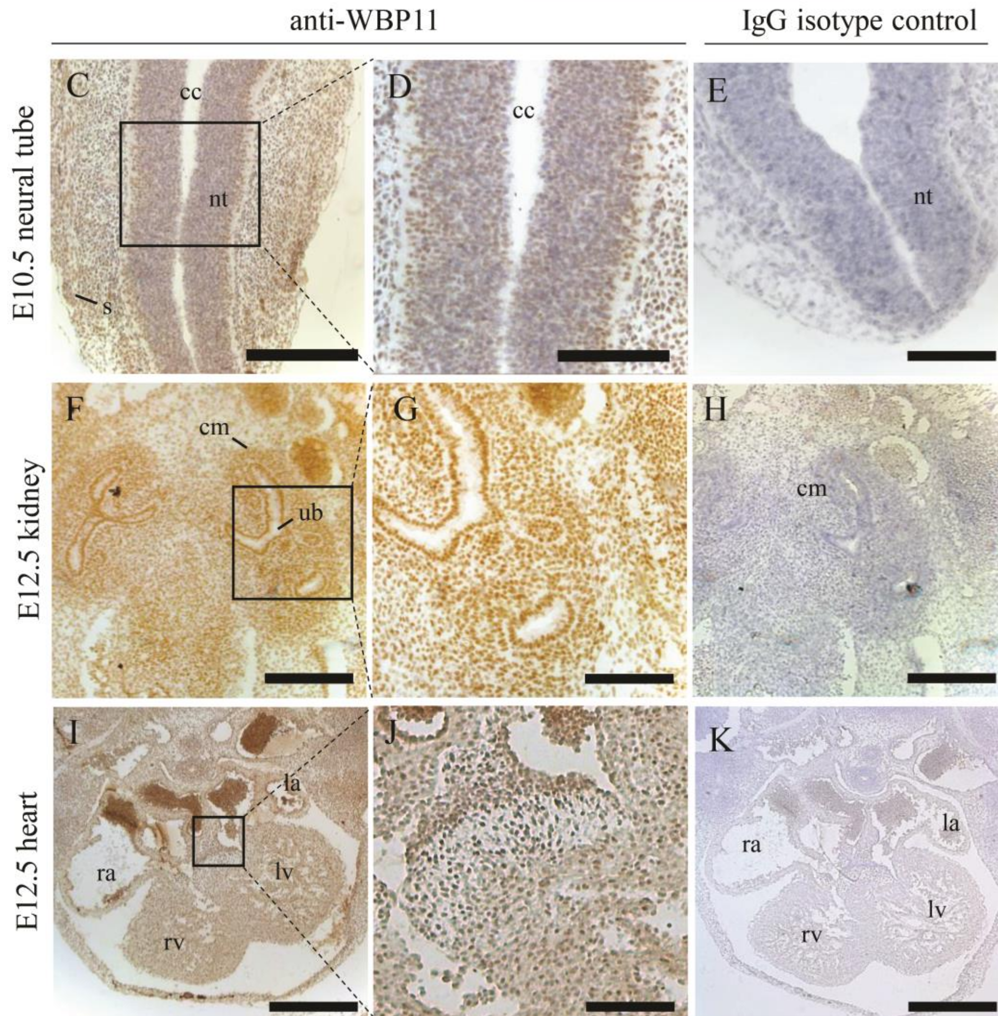

Downloaded from https://academic.oup.com/hmg/advance-article/doi/10.1093/hmg/ddaa258/6020188 by Bodleian Law Library user on 07 December 2020

Patient	1A	1B	2	3	4	4A	4B	4C	4D
WBP11 variant NM_016312.2	c.280C>T p.(Arg94Ter)	c.280C>T p.(Arg94Ter)	c.484C>T p.(Gln162Ter)	c.1559dup p.(Gly521TrpfsTer28)	c.688C>T p.(Arg230Ter)	c.688C>T p.(Arg230Ter)	c.688C>T p.(Arg230Ter)	c.688C>T p.(Arg230Ter)	c.688C>T p.(Arg230Ter)
Inheritance	Maternal		*De novo*	*De novo*	U	Maternal			
Gender	M	M	F	M	F	M	M	F	F
Growth	Birth at 40 WG, W: 2.67kg (-2 SD). Short stature	Birth at 42 WG, W: 3.69kg (-0.2 SD)	W, H: U	History of short stature. Normal at 12 years 10 months, W: 35.1 kg (-1.4 SD), H: 143.1 cm (-1.7 SD)	H: 157 cm (-0.7 SD), HC: 52.5 cm (-2 SD).	TOP at 27 WG, W: ~-1 SD, H, HC: 0 SD	At 11 years, W: 0 SD, H: +1.5 SD, HC: -2 SD	Fetal death at 16 WG, HC: 0 SD	Birth at 28 WG, W: -1.6 SD, H: -1 SD, HC: -1.5 SD. At 2 years,W: -2.5 SD, H: -1.5 SD, HC: -2.5 SD. At 8 years, W -1.5 SD, H normal, HC -2 SD
Cardiac, 8/13	-	PS, resolved by age 7 years	VSD	TAPVR, VSD, vascular ring, abnormal subclavian artery morphology	U	Hypoplastic left ventricle. Small VSD. Single atrium with anomalous pulmonary venous drainage. BAV. Interrupted aortic arch.	-	Muscular VSD	Muscular VSD in infancy, resolved by age 1 year
Gastrointestinal, 7/13	-	-	-	TOF, OA. Duodenal atresia	U	TOF, OA	-	TOF, OA	TOF, OA. Persistent feeding difficulties
Vertebral, 6/13	C3-C4, C6-C7 block vertebrae; C5 spina bifida occulta; bilateral omovertebral bones from C5; mild spinal canal stenosis	T12 butterfly vertebra, congenital scoliosis	C6-C7 fused cervical vertebrae. T1, T4 butterfly vertebrae. Left T2 fused thoracic vertebra . Abnormality of the right upper	C1-C3, C4- C6 fused cervical vertebrae. T8 butterfly vertebra	U	U	U	U	Hypoplasia of first costal arch

UNCORRECTED MANUSCRIPT

Downloaded from https://academic.oup.com/hmg/advance-article/doi/10.1093/hmg/ddaa258/6020188 by Bodleian Law Library user on 07 December 2020

	at C4-C5 and C5-C6		ribs						
Other musculoskeletal, 5/13	Sprengel deformity suggested by scapular elevation	Mild pectus excavatum	-	-	U	-	Sprengel deformity. Reduced mobility of left shoulder	U	Sprengel deformity – right thoraco-scapular aplasia
Limb, 5/13	Clinodactyly of the 5th finger	-	-	Unilateral abnormality of radial rayand left thumb morphology;	Tapered fingers. Hypoplasia of the right thumb with absent phalangeal crease	Deviation of toes, hypoplasia of the toenails	Bilateral hypoplasia of the thumbs, camptodactyly of 5th fingers, unilateral camptodactyly of 3rd and 4th fingers	-	-
Renal, 5/13	Right enlarged kidney (mild)	-	-	-	U	-	U	Right renal agenesis; left small, pelvic kidney	Relatively small kidneys
Cerebral and/or neurodevelopmental, 4/13	-	Suspected ADHD	Microcephaly. DD	Mild ID	-	NR	-	NR	-
Craniofacial, 7/13	Facial asymmetry. Preauricular pit. Low posterior hairline; slightly webbed neck	Broad forehead; deeply set eyes	Choanal atresia	Submucous cleft palate. Velopharyngeal insufficiency. No facial dysmorphism	-	Low-set, dysplastic right ear. Retrognathia. Wide nose	Right preauricular skin tags, dysplastic and anteverted ears	-	Plagiocephaly. Asymmetric crying face
Other	Mega cisterna magna, normal variant. Decreased testicular size, resolved. History of delayed puberty. Café au lait spot on back	Hypopigmented macule on left arm	-	Cryptorchidism. Stable conductive hearing impairment. Low CD19, and CD8 cells, hypogammaglobulinemia; no recurrent infections	-	Hypertrichosis	-	-	-

UNCORRECTED MANUSCRIPT

Downloaded from https://academic.oup.com/hmg/advance-article/doi/10.1093/hmg/ddaa258/6020188 by Bodleian Law Library user on 07 December 2020

Patient	5	6	7	7A
WBP11 variant NM_016312.2	c.612del p.(Gly205ValfsTer19)	c.169A>G p.(Met57Val)	c.612del p.(Gly205ValfsTer19)	c.612del p.(Gly205ValfsTer19)
Inheritance	U	U	Presumed paternal	
Gender	M	F	F	F
Growth	U	W, H, HC: < - 2SD. At 23 months, H: 73cm (-4.9SD)	Birth at39 WG, W 2.498kg (-2SD) At age 11 years 9 months, W: 26 kg (-2.6SD), H: 129.8cm (-2.6SD), HC: 50cm (-2.4SD)	U
Cardiac, 8/13	U	ASD	PFO, VSD, PDA that resolved spontaneously	U
Gastrointestinal, 7/13	U	TOF, OA	TOF, OA	Duodenal atresia
Vertebral, 6/13	U	U	Abnormal L5 vertebra	U
Other musculoskeletal, 5/13	U	U	-	Sprengel deformity
Limb, 5/13	U	U	-	U
Renal, 5/13	Renal agenesis	Renal agenesis	-	U
Cerebral and/or neurodevelopmental, 4/13	U	-	Agenesis of the corpus callosum, ventriculomegaly on head ultrasound at birth. Global DD, learning difficulties, ADHD	U
Craniofacial, 7/13	U	-	-	U
Other	-	Right inguinal hernia		U

Table 1: Heterozygous predicted damaging *WBP11* variants identified in patients with overlapping organ defects.

Total number of patients with defects indicated under each organ system, over total number of affected patients. F: female, M: male. +: present, -: no abnormality detected, NR: not relevant, U: unknown. W: weight, H: height/length, HC: head circumference, cm: centimetres, kg: kilograms, SD: standard deviation. C: cervical, T: thoracic, L: lumbar. ASD: atrial septal defect, BAV: bicuspid aortic valve, PDA: patent ductus arteriosus, PFO: patent

UNCORRECTED MANUSCRIPT

Downloaded from https://academic.oup.com/hmg/advance-article/doi/10.1093/hmg/ddaa258/6020188 by Bodleian Law Library user on 07 December 2020

foramen ovale, PS: pulmonic stenosis, TAPVR: total anomalous pulmonary venous return, VSD: ventricular septal defect. TOF: tracheo-oesophageal defect, OA: oesophageal atresia. ADHD: attention deficit hyperactivity disorder, DD: developmental delay, ID: intellectual disability. TOP: termination of pregnancy, WG: weeks of gestation.

UNCORRECTED MANUSCRIPT

Downloaded from https://academic.oup.com/hmg/advance-article/doi/10.1093/hmg/ddaa258/6020188 by Bodleian Law Library user on 07 December 2020

Variant Set	*P*-value
Set 1	0.01911
Set 2	0.02032

Table 2: Enrichment of *WBP11* variants in vertebral malformation cases

P-values for tests of *WBP11* variant enrichment in vertebral malformation cases (58 samples) over controls (194 samples). SNP-seq (Sequence) Kernel Association Test-Optimised (SKATO) was used for enrichment testing. Variants selected for gene enrichment had ExAC MAF < 0.01 (1%). Variant types selected were - Set 1: stop gain, frameshift (insertion/deletion), nonsynonymous SNV and splicing variants; Set 2: stop gain, frameshift (insertion/deletion) and variants that exceeded PolyPhen-2 HVAR score >=0.446 and CADD Phred score > 15.

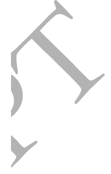

UNCORRECTED MANUSCRIPT

Downloaded from https://academic.oup.com/hmg/advance-article/doi/10.1093/hmg/ddaa258/6020188 by Bodleian Law Library user on 07 December 2020

Abbreviations

WBP11, WW Domain Binding Protein 11; RNP, ribonucleoprotein; LoF, Loss of Function; EJC, Exon Junction Complex; AP, anteroposterior; V, vertebral; A, anal; C, cardiac; TE, tracheo-oesophageal; R, renal; L, limb; NAD, nicotinamide adenine dinucleotide; CADD, combined annotation dependent depletion; HC, head circumference; SD, standard deviation; ID, intellectual disability; ADHD, attention deficit hyperactivity disorder; DD, developmental delay; SNV, single nucleotide variant; LoF, loss of function; IMPC, International Mouse Phenotyping Consortium; DQ, developmental quotient; IQ, intelligence quotient; MAF, minor allele frequency; BCA, bicinchononic acid; DMSO, dimethyl sulfoxide; PFA, paraformaldehyde; DAB, diaminobenzidine; micro-CT, micro-Computed-Tomography; PBS, phosphate buffered saline; NHMRC, National Health and Medical Research Council; F, female; M, male; +, present; -, no abnormality detected; NR, not relevant; U, unknown; W, weight; H, height/length; cm, centimetres; kg, kilograms;; C, cervical; T, thoracic; L, lumbar; ASD, atrial septal defect; BAV, bicuspid aortic valve; PDA, patent ductus arteriosus; PFO, patent foramen ovale; PS, pulmonic stenosis; TAPVR, total anomalous pulmonary venous return; VSD, ventricular septal defect; TOF, tracheo-oesophageal fistula; OA, oesophageal atresia; TOP, termination of pregnancy; WG, weeks of gestation

UNCORRECTED MANUSCRIPT

Downloaded from https://academic.oup.com/hmg/advance-article/doi/10.1093/hmg/ddaa258/6020188 by Bodleian Law Library user on 07 December 2020